Published in final edited form as:

Dev Cell. 2021 December 20; 56(24): 3380–3392.e9. doi:10.1016/j.devcel.2021.10.023.

MAR1 links membrane adhesion to membrane merger during cell-cell fusion in *Chlamydomonas*

Jennifer F. Pinello[1,3], **Yanjie Liu**[2,3], **William J. Snell**[1,2,*]

[1]Department of Cell Biology and Molecular Genetics, University of Maryland, College Park, Maryland 20742

[2]Department of Cell Biology, University of Texas Southwestern Medical Center, 6000 Harry Hines Boulevard, Dallas, TX 75390-9039, USA

[3]These authors contributed equally to this work.

Summary

Union of two gametes to form a zygote is a defining event in the life of sexual eukaryotes, yet the mechanisms that underlie cell-cell fusion during fertilization remain poorly characterized. Here, in studies of fertilization in the green alga, *Chlamydomonas*, we report identification of a membrane protein on *minus* gametes, Minus Adhesion Receptor 1 (MAR1), that is essential for the membrane attachment with *plus* gametes that immediately precedes lipid bilayer merger. We show that MAR1 forms a receptor pair with previously identified receptor FUS1 on *plus* gametes, whose ectodomain architecture we find is identical to a sperm adhesion protein conserved throughout plant lineages. Strikingly, before fusion, MAR1 is biochemically and functionally associated with the ancient, evolutionarily conserved eukaryotic class II fusion protein HAP2 on *minus* gametes. Thus, the integral membrane protein MAR1 provides a molecular link between membrane adhesion and bilayer merger during fertilization in *Chlamydomonas*.

eTOC blurb

Gamete fusion in organisms across kingdoms depends on fusogen HAP2. Pinello et al. demonstrate that receptor MAR1 is associated with HAP2 on *Chlamydomonas minus* gametes and binds to conserved adhesion protein FUS1/GEX2 on *plus* gametes, suggesting a mechanism that ensures bilayer merger is triggered only upon lineage-specific gamete membrane attachment.

Graphical Abstract

*Corresponding author and lead contact: wsnell1@umd.edu.

Author Contributions: J.F.P., Y.L., and W.J.S. designed the experiments. J.F.P. and Y. L. performed the experiments. J.F.P., Y.L., and W.J.S. analyzed the results and prepared the manuscript.

Declaration of Interests: The authors declare no competing interests.

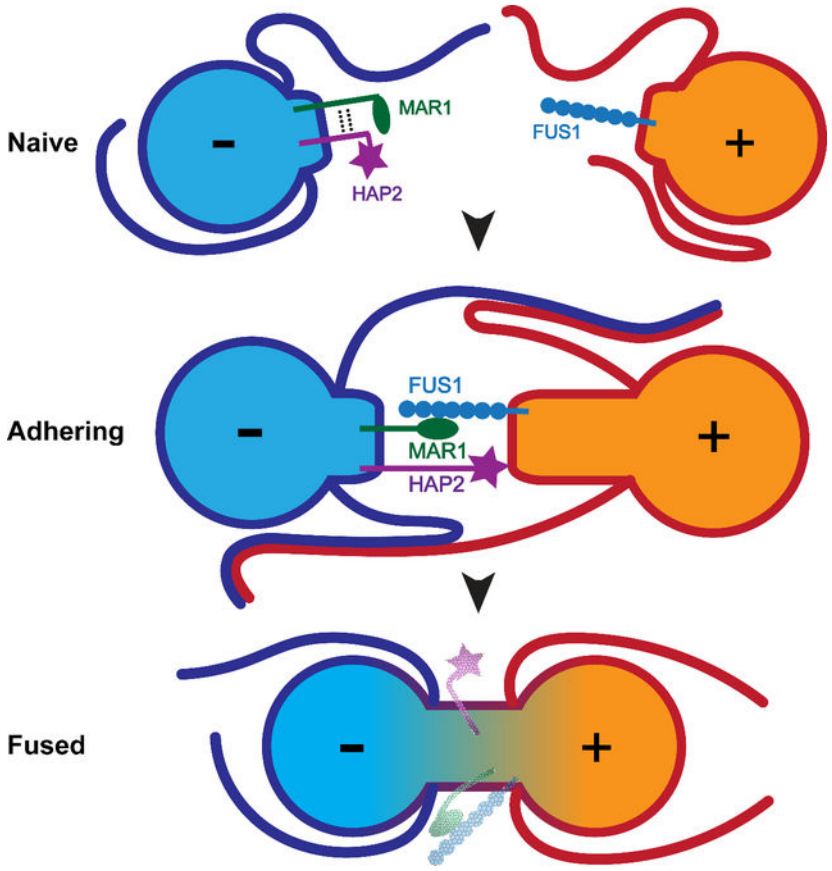

Keywords

membrane fusion reaction; gamete adhesion; cell-cell fusion; MAR1; FUS1; GEX2; HAP2; *Chlamydomonas* ; mating structure; fertilization; gamete fusion

Introduction

Fusion of gametes to form a zygote during fertilization is a complex cell-cell interaction whose core cellular features have been conserved since the origin of eukaryotes. Initial cell-cell recognition, typically at cell surface locations entirely separate from the site of fusion, bring the two gametes together and induce signals within them to prepare for fusion (Dean, 2007; Dresselhaus et al., 2016; Ikawa et al., 2010; Snell and Goodenough, 2009). Upon the consequent gamete activation, the gametes undergo a second interaction by gamete-specific adhesion proteins at newly available sites on their plasma membranes specialized for fusion. Attachment of the plasma membranes is rapidly followed by merger of the lipid bilayers to complete the fusion reaction. The conservation of the cellular steps of fertilization suggests that at least some of the molecular underpinnings of the gamete membrane fusion reaction might also be conserved (Sankaranarayanan and Higashiyama, 2018; Tajima and Nishimura, 2018). Surprisingly, in spite of over a century of study of fertilization (Bianchi and Wright, 2020; Lillie, 1914), we still lack a comprehensive understanding in any single organism of the molecules or mechanisms that compose and regulate the gamete fusion reaction.

Studies in mouse have shown that the proteins IZUMO1 on sperm and JUNO on the egg form a complex that is essential for the sperm-egg membrane binding preceding fusion. The two proteins, which form the only receptor pair known to be essential for gamete membrane adhesion in any organism, are insufficient for fusion and a chordate gamete fusogen remains unidentified (Aydin et al., 2016; Bianchi et al., 2014; Inoue et al., 2005; Ohto et al., 2016). Several other mouse gamete proteins with mammalian orthologs have been reported as essential for fertilization, including CD9 on eggs (Le Naour et al., 2000; Miyado et al., 2000), and FIMP (Fujihara et al., 2020), SPACA6 (Barbaux et al., 2020; Lorenzetti et al., 2014), SOF1 (Noda et al., 2020), and TMEM95 (Lamas-Toranzo et al., 2020; Noda *et al.*, 2020) on sperm, but they neither adhere nor fuse cells when heterologously expressed, and their molecular functions remain unclear.

Proteins with roles in gamete membrane interactions during the fusion reaction have been described in several other model organisms, including Prm1p in *S. cerevisiae* (Heiman and Walter, 2000); Spe-9, Spe-45, and EGG-1 & 2 in *C. elegans* (Kadandale et al., 2005; Nishimura et al., 2015; Singaravelu et al., 2015; Singson et al., 1998); P48/45, p47 and p230 in the malaria pathogens *Plasmodium* (van Dijk et al., 2010); the mating type proteins in ciliates (Cervantes et al., 2013); Bouncer in *D. rerio* (Herberg et al., 2018); GEX2 and DMP8 & 9 in the plant *Arabidopsis thaliana* (Cyprys et al., 2019; Engel et al., 2005; Mori et al., 2014; Takahashi et al., 2018); and FUS1 in the green alga *Chlamydomonas reinhardtii* (hereafter, *Chlamydomonas*) (Ferris et al., 1996; Misamore et al., 2003). The presence of immunoglobulin-like (Ig-like) domains in Spe-45, IZUMO1, GEX2, and FUS1 is consistent with the known roles of the domain in protein-protein interactions. This collection of adhesion proteins, however, has not been reported to possess a common overall domain architecture, and thus, a gamete adhesion protein family that spans unicellular and multicellular plants or animals has been absent.

In contrast, a single protein of conserved structure, HAP2, is essential for fertilization in unicellular and multicellular organisms across kingdoms, and was likely the primordial sexual fusogen (Camacho-Nuez et al., 2017; Cole et al., 2014; Ebchuqin et al., 2014; Hirai et al., 2008; Johnson et al., 2004; Liu et al., 2008; Mori et al., 2006; Okamoto et al., 2016; Ramakrishnan et al., 2019; Steele and Dana, 2009). Studies in *Chlamydomonas, Plasmodium,* and *Tetrahymena* showed that HAP2 was dispensable for gamete membrane adhesion but was required for bilayer merger (Cole *et al.*, 2014; Liu *et al.*, 2008). Remarkably, structural modeling and X-ray crystallography demonstrated an unambiguous structural homology between HAP2 and viral and developmental class II fusion proteins, including the envelope proteins from the *Bunyavirales*, *Flaviviruses,* and *Alphaviruses* and EFF-1 from *C. elegans* (Fedry et al., 2017; Perez-Vargas et al., 2014; Pinello et al., 2017; Valansi et al., 2017). More recent studies showed that *Chlamydomonas* HAP2, which is required only on *minus* gametes, indeed forms trimers in vivo and that trimer formation is essential for fusion (Zhang et al., 2021). Notably, HAP2 (also called GCS1) has not yet been detected in fungi or chordates, either because it was lost or because it evolved to become unrecognizable.

In *Chlamydomonas*, when *plus* and *minus* gametes are mixed together, they initially recognize and adhere to each other by their cilia through mating type-specific adhesion

proteins that function only on the cilia, SAG1 in *plus* gametes and SAD1 in *minus* gametes (Snell and Goodenough, 2009) (Fig. 1A). Ciliary adhesion activates a protein kinase-dependent signaling pathway that leads to increases in intracellular cyclic AMP, thereby triggering gamete activation. During activation, gametes release their extracellular matrices (cell walls), recruit additional adhesion proteins to their ciliary membranes (Belzile et al., 2013; Ranjan et al., 2019), and assemble a membrane protuberance called a mating structure between their two cilia (Friedmann et al., 1968; Weiss et al., 1977). Ciliary adhesion and the accompanying vigorous motility of the cells bring the apical ends of pairs of gametes into alignment, leading to collisions between the two mating structures and adhesion of their tips. FUS1 is the *plus* gamete-specific membrane adhesion protein present on the mating structures of *plus* gametes, and *plus* gametes lacking FUS1 fail to adhere, fail to support formation of HAP2 trimers, and fail to fuse (Ferris *et al.*, 1996; Misamore *et al.*, 2003; Zhang *et al.*, 2021). Within seconds of membrane adhesion, HAP2 present on the *minus* mating structure engages with the lipid bilayer of the *plus* mating structure to fuse the two membranes (Feng et al., 2018; Zhang *et al.*, 2021), followed by rapid coalescence of the two gametes into a quadri-ciliated zygote (Fig. 1A). Nuclear fusion by the protein, GEX1, which is a member of the KAR5/GEX1 family of nuclear fusion proteins, follows soon thereafter (Beh et al., 1997; Engel *et al.*, 2005; Ning et al., 2013).

Here, we report that *Chlamydomonas* FUS1 and previously described plant sperm adhesion protein, GEX2, are members of a broadly conserved protein family characterized by extracellular domains composed almost entirely of Ig-like domains. We identify a new, lineage-restricted protein on *minus* gametes, MAR1, that is a receptor for FUS1 on *plus* gametes. Formation of the FUS1-MAR1 pair is essential for the gamete membrane attachment that immediately precedes bilayer merger and is necessary for gamete fusion. Moreover, we find that MAR1 is biochemically associated with HAP2 and is required for proper HAP2 expression and localization at the *minus* mating structure. Thus, during the gamete membrane fusion reaction in *Chlamydomonas*, a lineage-specific protein, MAR1, functions at the nexus of conserved membrane adhesion protein, FUS1, and ancient membrane fusogen, HAP2.

Results

Chlamydomonas FUS1 and plant gamete adhesion protein, GEX2, share a common ectodomain architecture

We used the more powerful protein analysis methods available now to update the earlier report that the FUS1 ectodomain contained 5 Ig-like domains (Misamore *et al.*, 2003). Our new analysis uncovered FUS1 orthologs in several other algal species (Yamamoto et al., 2021) and identified two more Ig-like domains in FUS1, for a total of 7 (Fig. 1B and Table S1). To our surprise, DELTA-BLAST, PSI-BLAST, and PROMALS3D analyses identified sequence and secondary structure similarities between the entire ectodomains of *Chlamydomonas* FUS1 and plant GEX2 sequences (including those of *Arabidopsis thaliana*, *Oryza sativa,* and *Triticum dicoccoides*; Table S1 and Data S1). Furthermore, in an HHPred query of the *A. thaliana* proteome with the FUS1 ectodomain, GEX2 was the top hit (E-

value: 2.2e-13, Identities: 15%) and in an HHPred query of the *Chlamydomonas* proteome with the GEX2 ectodomain, FUS1 was the top hit (E-value: 8.7e-26, Identities: 16%).

Structural modeling using the coevolution-independent modeler, RaptorX contact prediction (Xu et al., 2021), showed similar tertiary structures for *Chlamydomonas* FUS1 and *Arabidopsis* GEX2 ectodomains (Fig. 1B and Table S1). Template-based homology modeling on all platforms tested (PHYRE2, SWISS-MODEL and HHPRED) found that *Chlamydomonas* FUS1 and *Arabidopsis* GEX2 have strong structural homologies to the same structures in the protein data bank, namely, the *Dictyostelium* gelation factor rod domain and bacterial invasin-intimin-like proteins, thereby demonstrating structural uniformity among their Ig-like domains (Fig S1). Taken together, our results indicate that FUS1 and GEX2 belong to a family of gamete cell surface adhesion proteins whose ectodomains are constituted by Ig-like domains.

A *minus* gamete protein that binds to FUS1

We took advantage of the ease of preparing biochemical quantities of pure gametes in *Chlamydomonas* to identify proteins on *minus* [*(−)*] gametes that bound to FUS1 on *plus* [*(+)*] gametes. *hap2(−)* gametes were surface labeled with biotin, mixed with *fus1*::*FUS1-HA(+)* gametes, and immunoprecipitation, immunoblotting, and mass spectrometry were used to identify biotinylated *minus* gamete proteins that associated with FUS1-HA. Use of the fusion-defective *hap2(−)* gametes to block fertilization at the stage of mating structure adhesion maximized opportunities for adhesion protein interactions and prevented the degradation of FUS1 that is coincident with gamete fusion (Liu et al., 2010). As a control, we also mixed biotinylated *hap2(−)* gametes with *fus1(+)* gametes, which lack FUS1. FUS1-HA was pulled down efficiently by anti-HA antibody, and as expected, staining was absent in the *fus1* control samples (Fig. 1C, left panel). Importantly, streptavidin blotting showed a biotinylated protein migrating with an apparent molecular mass of ~250 kDa that was co-immunoprecipitated only in the FUS1-HA-containing sample (Fig. 1C, right panel).

Specific expression of Cre03.g176961 in *minus* gametes

The protein encoded by gene *Cre03.g176961* exhibited high coverage in mass spectrometry analysis of the 250 kDa region of samples from FUS1 immunoprecipitates and was absent in *fus1* samples (Data S2). Importantly, previous gene expression studies in *Chlamydomonas* vegetative cells and naive and activated gametes (Ning *et al.*, 2013) showed that *Cre03.g176961* transcripts were uniquely present in *minus* gametes and upregulated upon activation (Fig. 1D). This expression signature is similar to that of other fertilization-essential transcripts in *minus* gametes (Ning *et al.*, 2013), including *HAP2*, and distinct from those of *plus*-specific *FUS1* and constitutively expressed ribosomal transcript *RPL4* (Fig. 1D), making the Cre03.g176961 protein, hereafter called *Minus* Adhesion Receptor 1 (MAR1), a strong candidate for a FUS1 binding partner.

Based on the annotation in Phytozome (Goodstein et al., 2012), and confirmatory RT-PCR characterization of the transcript, *MAR1* (GenBank: KT288268) encodes a 1018-residue, single-pass transmembrane protein with a predicted molecular mass of 99 kDa. Analysis of the amino acid sequence predicted a signal peptide, a 365-residue ectodomain, a single

transmembrane domain, and a 608-residue cytoplasmic domain (Fig. 1E; scale-drawing of FUS1 shown for comparison). Two notable features of the MAR1 ectodomain are a growth factor receptor cysteine-rich domain near the N-terminus (residues 78–159) and a proline-rich segment (residues 142 to 365) that includes 5 repeats of a "PPSPX" motif. The latter motif was previously identified in other *Chlamydomonas* proteins, including a cell wall protein, GP1 (Ferris et al., 2001); and the ciliary adhesion proteins, SAG1 and SAD1 (Ferris et al., 2005). In the MAR1 cytoplasmic domain, structural homology searches found segments with likeness to the ABA receptor kinase from *Arabidopsis* (PDB: 5XD6, residues 512–620), and collagen (PDB: 1YGV, residues 619–1018). Detectable MAR1 sequence homologies in other organisms, however, were scant, with only a small number of algal relatives containing putative MAR1 orthologs (Data S2).

We introduced a FLAG-tagged MAR1 transgene driven by its endogenous promoter into *hap2(−)* cells, and *hap2*::*HAP2-HA(−)* cells. The MAR1-FLAG protein was expressed in *minus* gametes and absent in *minus* vegetative cells (Fig. 2A). Consistent with the biotinylation studies, and in spite of a predicted molecular mass of 107 kDa, MAR1-FLAG appeared as a ~250 kDa protein in SDS-PAGE. We are uncertain of the basis for this anomalous behavior, but the several proline-rich regions might contribute to its altered migration pattern (Ferris *et al.*, 2001). Immunoblot analyses of lysates from equal numbers of transgene-expressing gametes indicated that the three gamete-specific proteins, MAR1, HAP2 and FUS1, were expressed at similar levels (Data S2).

MAR1 is a receptor for FUS1

In vivo and in vitro protein interaction assays were consistent with the biotinylation results and showed that MAR1 and FUS1 bound to each other. In in vivo assays with live cell mixtures, *fus1::FUS1-HA(+)* gametes were mixed with *hap2::MAR1-FLAG(−)* gametes for 30 minutes to allow gamete activation and mating structure adhesion without membrane fusion, followed by disruption of the samples in lysis buffer, immunoprecipitation with anti-FLAG antibody, and immunoblotting with anti-HA antibody. *hap2(−)* gametes (i. e., expressing only un-tagged endogenous MAR1) mixed with *fus1::FUS1-HA(+)* gametes were used as a control. As shown in Fig. 2B, FUS1-HA was present in the FLAG immunoprecipitates of the *hap2::MAR1-FLAG(−)* gametes that had been mixed with *fus1::FUS1-HA(+)* gametes, but not in the control immunoprecipitates. Related experiments, in which separately prepared detergent lysates of activated *hap2::MAR1-FLAG(−)* gametes and *fus1::FUS1-HA(+)* gametes were mixed together followed by immunoprecipitation and immunoblotting as above, also showed that the two proteins were associated with each other (Fig. 2C). Additional experiments with lysates of cells expressing IFT172-FLAG mixed with FUS-HA lysates and with lysates of cells expressing IMP3-HA mixed with MAR1-FLAG lysates demonstrated the specificity of the interaction between MAR1-FLAG and FUS1-HA (Fig. S2). Finally, we found that bacterially expressed, His-tagged MAR1 ectodomain (His-MAR1) was precipitated by the GST-tagged FUS1 ectodomain (rFUS1) but not by GST alone (Fig. 2D). Together, these results demonstrated that the ectodomains of MAR1 and FUS1 directly interacted with each other.

Mating structure adhesion is severely impaired in *mar1 minus* gametes and fusion is blocked

To test whether the MAR1 and FUS1 interaction detected biochemically was important functionally, we examined the fertilization phenotypes of a *Chlamydomonas* CLiP library mutant *minus* strain, *LMJ.RY0402.185187* (hereafter, called *mar1*), which is annotated to have an insertion in the *MAR1* gene (Li et al., 2019). PCR across the predicted insertion site showed that the *CIB1* plasmid had indeed inserted into the 3rd exon of *MAR1*, thereby disrupting its coding sequence (Fig. 3A, Fig. S3). The *mar1(−)* mutant cells showed no detectable morphological or growth phenotype when cultured as vegetative cells. Furthermore, when placed into N-free medium overnight, the *mar1(−)* cells differentiated into *minus* gametes that were fully capable of ciliary adhesion with wild type (WT) *plus* gametes upon mixing, forming characteristic, large clusters of *plus* and *minus* gametes adhering to each other by their cilia (Fig. 3B low magnification DIC images; Fig. 3C SEM image). Gamete activation, as quantitatively assessed by cell wall loss, was also indistinguishable in mixtures of *mar1(−)* gametes or WT*(−)* control gametes with WT*(+)* gametes (Fig. 3B, bottom).

mar1(−) gametes, however, were severely impaired in their ability to undergo mating structure adhesion with WT*(+)* gametes. Whereas a mean of 56% of cells adhered by their mating structures in the fusion-blocked mixtures of *hap2(−)* gametes with WT*(+)* gametes, only 6% adhered in the mixtures of *mar1(−)* gametes with WT*(+)* gametes. This adhesion-defective phenotype was indistinguishable from that observed in mixtures of WT*(−)* gametes mixed with *fus1(+)* gametes (Fig. 3D and Misamore *et al.*, 2003). Introduction of the *MAR1-FLAG* transgene into *mar1(−)* gametes also harboring the *hap2* gene-disruption, rescued mating structure adhesion with WT*(+)* gametes to levels analogous to that of mixtures of *hap2(−)* and WT*(+)* gametes. These results demonstrated a central role for MAR1 in mating structure adhesion.

Notably, and mirroring the phenotypes observed in both the adhesion-defective *fus1(+)* gametes (Ferris *et al.*, 1996; Misamore *et al.*, 2003) and fusion-defective *hap2(−)* gametes, loss of MAR1 completely abrogated gamete fusion as quantified by counts of quadri-ciliated zygotes at 10–30 min after mixing (Fig. 3E, 10 min results) and by visual examination after overnight incubation to detect appearance of immotile zygotes, which appear as heterogeneous, green flocculant material in liquid cultures (Fig. 3F). The fusion defect of *mar1(−)* gametes was rescued with the *MAR1-FLAG* transgene (Fig. 3E, F), and the extent of fusion 10 minutes after mixing *mar1;MAR1-FLAG*(−) gametes with WT*(+)* gametes (77% fusion) was indistinguishable from that in mixtures of WT gametes (75% fusion), consistent with the results of the macroscopic assay (Fig. 3F). As expected, and demonstrating that MAR1 functions only in *minus* gametes during fertilization, *plus* gametes bearing the *mar1* mutation were fully competent to fuse with WT*(−)* gametes (61%). These results showed that MAR1 was essential in *minus* gametes for zygote formation.

Furthermore, analysis of F_1 and F_2 progeny from crosses of *MAR1-FLAG*-rescued *mar1(−)* gametes mixed with *plus* gametes (Fig. S3) confirmed that the adhesion- and fusion-defective phenotypes of *mar1(−)* gametes co-segregated with the *mar1* mutant genotype. As

expected, crosses of *mar1(−)* gametes with WT*(+)* gametes failed to produce any progeny. Taken together, our biochemical and genetic results demonstrated that the direct interaction of mating structure membrane proteins MAR1 on *minus* gametes and FUS1 on *plus* gametes mediated the membrane attachment between the two gametes that occurs after their mutual recognition and activation, and that formation of this receptor pair was essential for the gamete membrane fusion reaction.

MAR1-FLAG is localized at the *minus* mating structure and is lost rapidly after gamete fusion

Confirming that MAR1 functions at the cell surface, brief incubation of live *hap2::MAR1-FLAG;HAP2-HA(−)* gametes with pronase resulted in loss of nearly all of MAR1-FLAG (Fig. 4A, top), and as expected, only the surface-expressed upper isoform (S) of HAP2 (Fig. 4A, middle, Liu *et al.*, 2008). Immunostaining of *mar1;MAR1-FLAG;hap2;HAP2-HA(−)* gametes with anti-FLAG antibodies further showed that MAR1-FLAG was present as a punctum between the two cilia at the apical ends of the *minus* gametes (Fig. 4B), the location of the *minus* mating structure. MAR1-FLAG remained localized at the *minus* mating structure after gamete activation (Fig. S4). Double immunostaining of *mar1;MAR1-FLAG;hap2;HAP2-HA(−)* gametes with anti-HA and anti-FLAG antibodies further confirmed their co-localization at the *minus* mating structure (Fig. 4C). Finally, similar to loss of HAP2 and FUS1 after fusion, and as part of a block to polygamy (Liu *et al.*, 2010), 30 minutes after ~70% of *mar1::MAR1-FLAG(−)* gametes had fused with WT*(+)* gametes, MAR1-FLAG had become nearly undetectable (Fig. 4D).

Biochemical and functional assays demonstrate an association between MAR1 and fusogen HAP2

To test for a biochemical interaction between these temporally co-functioning, co-localized proteins, we immunoprecipitated MAR1-FLAG from the lysates of activated *minus* gametes expressing both MAR1-FLAG and HAP2-HA and used immunoblotting to assess whether HAP2-HA was also present in the immunoprecipitates. As shown in Fig. 4E, HAP2-HA was indeed present in the anti-FLAG immunoprecipitates, but absent in control immunoprecipitates from activated *hap2::HAP2-HA(−)* gametes (lacking MAR1-FLAG), and activated *mar1; MAR1-FLAG(−)* gametes (lacking HAP2-HA). Notably, we consistently found that MAR1 preferentially associated with the upper, membrane-surface-expressed isoform (S) of HAP2 (Fig. 4E). Despite the association, MAR1-FLAG expression (Fig. 5A) and localization (Fig. 5B) in *hap2(−)* gametes were indistinguishable from that of *minus* gametes expressing WT HAP2-HA. Furthermore, as reported here (Fig. 3D) and previously (Feng *et al.*, 2018; Liu *et al.*, 2008; Zhang *et al.*, 2021), *hap2(−)* gametes were fully capable of undergoing mating structure adhesion with *plus* gametes. Thus, MAR1 expression, localization, and function were independent of HAP2.

On the other hand, the expression and localization of HAP2 in *minus* gametes lacking MAR1 were substantially altered. Total HAP2 protein expression in *mar1;HAP2-HA(−)* and *mar1::HAP2-FLAG(−)* gametes was reduced 2-fold compared to that of strains expressing HAP2 in a WT *MAR1* background (representative blots, Fig. 5C and Fig. S5; quantification of multiple independent experiments, Fig. 5D). Moreover, quantitative

densitometry measurements of immunoblots across multiple biological replicates also showed that the mean percentage of HAP2 present in the upper, surface-expressed isoform was reduced from 50% in WT*(−)* gametes to 36% in the *mar1(−)* gametes, representing a reduction of 28% (Fig. 5E; Fig. S5).

Absence of MAR1 also substantially altered HAP2 localization. Immunofluorescent staining and confocal microscopy of HAP2-HA in *minus* gametes containing WT MAR1 showed that the predominant localization of HAP2-HA was, as shown above (Fig. 4C) and previously (Fedry *et al.*, 2017; Feng *et al.*, 2018; Liu *et al.*, 2010; Zhang *et al.*, 2021), as a single spot at the site of the *minus* mating structure (Fig. 5F, middle panel, Fig. S5). Low intensity, non-specific anti-HA staining was observed in negative control WT*(+)* gamete samples (Fig. 5F, left panel), as well as in small amounts within cells and elsewhere on the slide in other samples (as shown above in Figs. 4C). On the other hand, HAP2-HA localization in *minus* gametes lacking MAR1 was strikingly different. Consistent with the immunoblotting results, the immunofluorescence signal in *mar1(−)* gametes was much lower (Fig. S5) and was only infrequently detected as a single apically-localized spot. Fig. 5F, right panel shows an image whose relative brightness was increased to allow visualization of the cellular localization of this reduced amount of HAP2-HA. Often, HAP2-HA in the *mar1(−)* gametes appeared as smaller puncta close to the site of the mating structure, but was predominately found throughout the cell body as multiple, discrete puncta of varying sizes (Fig. 5F, Fig. S5). Thus, proper expression and localization of HAP2-HA at the *minus* mating structure depended upon MAR1.

Discussion

We investigated the proteins and protein interactions that underlie membrane adhesion and bilayer merger during the gamete membrane fusion reaction in *Chlamydomonas*. We determined that the ectodomain of FUS1, the previously identified adhesion protein on the *plus* gamete mating structure, is predicted to be constituted entirely by a linear array of Ig-like domains, a domain architecture that BLAST searches and structural modeling show is similar to that of GEX2, a gamete adhesion protein present throughout land plants. We also identified a lineage-restricted, *minus* gamete-specific membrane protein, MAR1, that is localized at the surface of the *minus* mating structure and that binds directly to FUS1. Like FUS1, MAR1 is essential for mating structure adhesion and for gamete fusion. These interacting proteins are now the second gamete membrane adhesion receptor pair demonstrated to be essential for fertilization (Bianchi *et al.*, 2014). In addition to interacting with FUS1, MAR1 is also associated with HAP2 on *minus* gametes and essential for proper HAP2 expression and localization during gametogenesis. Our results suggest that the membrane adhesion immediately preceding HAP2-dependent bilayer merger during fertilization in organisms across Viridiplantae is mediated by an interaction between a member of the conserved FUS1/GEX2 family of adhesion proteins and a lineage-restricted binding partner on the cognate gamete.

FUS1/GEX2 joins HAP2 and KAR5/GEX1 to make a trio of protein families central to sexual reproduction in organisms from unicellular green algae to flowering plants

The Immunoglobulin Superfamily (IgSF) is large and diverse, and many of its members function in intercellular adhesion in prokaryotes and eukaryotes (Chatterjee et al., 2020; Honig and Shapiro, 2020). Several proteins important for sperm-egg interactions in metazoans possess Ig-like domains (Nishimura and L'Hernault, 2016), the best characterized being the sperm adhesion protein IZUMO1, whose single Ig-like domain forms a portion of the interface between IZUMO1 and its egg binding partner, JUNO (Aydin *et al.*, 2016; Ohto *et al.*, 2016). The previously reported presence of Ig-like domains in *Chlamydomonas* FUS1 (Misamore *et al.*, 2003) and plant GEX2 (Mori *et al.*, 2014) called further attention to the widespread use these domains in sexual reproduction. Our findings here indicate, however, that the Ig-like domains constitute the entire functional portion of FUS1 and nearly the entire ectodomain of GEX2. The expansive binding repertoire of vertebrate antibody proteins, which are composed entirely of immunoglobulin domains, is provided by structural variations in a subset of their domains. Future structural studies should provide insights into whether similar variations in particular Ig-like domains of FUS1/GEX2 family members underlie their ability to interact with gamete receptor proteins across taxa.

Remarkably, uncovering the breadth of conservation within this family of gamete adhesion proteins now indicates that at least three of the core functions unique to eukaryotic sexual reproduction are carried out by three protein families conserved across all plant lineages: (1) gamete membrane adhesion mediated by FUS1/GEX2 family members, (2) membrane merger mediated by HAP2 family members, and (3) pronuclear fusion mediated by the KAR5/GEX1 family of nuclear envelope proteins (Mori *et al.*, 2014; Ning *et al.*, 2013; Wong and Johnson, 2010). The HAP2 and KAR5/GEX1 families are not restricted to plant lineages and are essential for sexual reproduction in organisms from green algae and protists to multicellular plants and animals. The conservation of domain architectures within members of each of these three families suggests that while the evolutionary pressures on reproductive proteins often lead to rapid changes in their primary amino acid sequences, this diversification may take place on a relatively unchanging structural backbone (Ferris et al., 1997; Mori *et al.*, 2014; Swanson and Vacquier, 2002).

MAR1 is bifunctional and interacts with FUS1 on *plus* gametes and HAP2 on *minus* gametes during the membrane fusion reaction

Our biochemical results with endogenous proteins in gamete lysates and with bacterially expressed proteins indicated that interaction between FUS1 and MAR1 ectodomains was independent of *Chlamydomonas*-specific post-translational modifications and that it was direct. One potential binding site in the MAR1 ectodomain could be within its proline-rich region, which contains several PPSPX repeats akin to the poly-proline repeats of algal and higher plant hydroxyproline-rich glycoproteins (HPRGs, Ferris *et al.*, 2005; Ferris *et al.*, 2001) that support other types of protein-protein interactions. The MAR1 growth factor receptor domain, which is similar to growth factor motifs found in other gamete interaction proteins such as a mating type protein in the ciliate, *T. thermophila* (Cervantes *et al.*, 2013); and Spe-9 in *C. elegans* (Singson *et al.*, 1998), could also be a potential protein interaction site.

Furthermore, results from several independent methods were all consistent with a biochemical and functional association between MAR1 and the class II fusogen HAP2 on the *minus* mating structure. Total HAP2 expression as well as the portion of HAP2 at the cell-surface were reduced in *minus* gametes lacking MAR1, HAP2 was mis-localized in gametes lacking MAR1, and MAR1 was biochemically associated with the cell-surface form of HAP2. One interpretation of these findings is that, like the partner protein interactors of viral class II fusion proteins, MAR1 participates in biosynthesis and trafficking of HAP2 to the *minus* mating structure. For example, in the absence of their partner E2 proteins, the E1 fusogens of Sindbis virus and Semliki Forest Virus are inefficiently transported to the plasma membranes of their host cells (Andersson et al., 1997; Carleton et al., 1997). Independently of a role in trafficking, MAR1 might also stabilize HAP2 at the mating structure.

It will be important to determine whether the MAR1-HAP2 association is direct or indirect and to identify the regions of MAR1 and HAP2 that participate in this association. If the interaction is indirect, a handful of *Chlamydomonas* membrane proteins whose transcripts show *minus* gamete-specific expression similar to MAR1 (Ning *et al.*, 2013) would be good candidates for a linking protein; including Cre03.g175926, which has some sequence similarity to MAR1. If the interaction is direct, possible cytoplasmic domain interaction sites within HAP2 and MAR1 are a 237-residue segment of HAP2 essential for its mating structure localization (Liu et al., 2015) and a 400-residue segment within MAR1 with a predicted structural likeness to collagen.

Before a structure was available, Wong et al. (2010) demonstrated that the fusion capacity of *Arabidopsis* HAP2 was retained when its ectodomain was exchanged with the HAP2 ectodomain from a closely related species, but was not when the swap was with the ectodomain of a more distantly related species, indicating that the ectodomain of HAP2 was important in lineage-specific functions. Recent protein structures of the *Chlamydomonas* trimeric HAP2 ectodomain have brought to light regions within loops of domain I that may participate in such lineage-specific protein-protein interactions (Baquero et al., 2019; Feng *et al.*, 2018). Furthermore, comparisons between the HAP2 structures of *Chlamydomonas*, *Arabidopsis*, and *Trypanosoma cruzi* showed substantial, taxa-specific differences in their fusion loops, supporting a possible lineage-specific role for protein interactions of this region (Fedry et al., 2018).

Our discovery that the lineage-specific protein MAR1 functions at the nexus of two broadly conserved, fusion-essential protein families leads to the speculation that the cognate gamete adhesion receptor pairs in other organisms might also be composed of one conserved protein and another that is lineage specific. The IZUMO1-JUNO receptor pair would support such a model, as JUNO is specific to mammals, but IZUMO1 is present throughout vertebrates (Bianchi *et al.*, 2014; Grayson, 2015). Even this model is overly simplistic, however, since the FUS1/GEX2 family member in *Chlamydomonas* is present in the gamete lacking HAP2, whereas the FUS1/GEX2 family members in land plants are present in the gamete expressing HAP2.

Nevertheless, our findings raise the exciting possibility that MAR1 binding to *Chlamydomonas* FUS1 triggers conformational changes within HAP2 required for its conversion to fusion-driving trimers (Zhang *et al.*, 2021). In class I fusogen-dependent Paramyxoviruses, the interaction of a fusogen-associated adhesion protein with its membrane receptor activates the fusion protein (Navaratnarajah et al., 2020). Future studies on the FUS1-MAR1-HAP2 axis have the potential to illuminate new, conserved regions in HAP2 that act before its function in bilayer merger in organisms across plant taxa as well as in the many unicellular organisms and metazoans that also depend on HAP2 for gamete fusion.

Limitations of the study

Given that FUS1 and HAP2 are each members of conserved protein families that function in the gamete membrane fusion reaction, it is possible that they also interact directly with each other. Such an interaction could be essential for the fusion reaction but would have gone undetected in these studies. Also, our studies were focused on the role of MAR1 in HAP2 cellular properties and functions before *plus* and *minus* gametes bind to each other at their mating structures, but our results are silent on whether FUS1 binding to MAR1 alters the MAR1-HAP2 interaction. In addition, MAR1 or the MAR1-HAP2 association might contribute to structural properties of the *minus* mating structure that are important for fusion but that can be determined by ultrastructural studies of cells or by structural studies with proteins expressed in vitro.

STAR Methods

RESOURCE AVAILABILITY

Lead contact—Further information and requests for resources and reagents should be directed to and will be fulfilled by the lead contact, Dr. William J. Snell (wsnell1@umd.edu)

Materials availability—Materials generated in this study including plasmids and new *Chlamydomonas* strains are available upon request from the lead contact or direct purchase from the *Chlamydomonas* Resource center (https://www.chlamycollection.org/).

Data and code availability

- All other data reported in this paper are available from the lead contact upon request.
- No large-scale datasets or new code were generated in this study.
- Any additional information required to reanalyze the data reported in this paper is available from the lead contact upon request.

EXPERIMENTAL MODEL AND SUBJECT DETAILS

Chlamydomonas cell culture—Cells were grown vegetatively in liquid TAP medium under a 13:11 h light-dark cycle at 22°C. Gametogenesis was induced by transferring vegetative cells into N-free medium followed by overnight agitation on a shaker in continuous light.

Chlamydomonas stocks—Existing *Chlamydomonas* strains used for experiments were *21gr(+)*, *fus1(+)*, *fus1::FUS1-HA(+)*, *hap2(−)*, *hap2::HAP2-HA(−)*, *CC-5313(+)*, *mar1(−)* also called *LMJ.RY0402.185187(−)*, and *CC-5325(−)*. Transgenic strains generated in this study and used for experiments were made by stable transformation and crosses of the above strains. The following transgenic *Chlamydomonas* strains were generated and are designated as follows by numeric or alphanumeric codes in brackets [with coded independently-isolated strains separated by commas] within the given genotypes: *mar1;MAR1-FLAG(+)* [3d-1]; *mar1::MAR1-FLAG(−)* [MF-c7]; *mar1;MAR1-FLAG(−)*[111,115,147]; *mar1(−)* [106, 133, 144]; *mar1;hap2(−)*[73; 98]; *mar1;hap2(+)*[148,156]; *mar1;hap2; MAR1-FLAG(−)*[78,146]; *mar1;HAP2-HA(−)*[122]; *mar1;hap2;HAP2-HA(−)*[132]; *mar1::HAP2-FLAG(−)*[HF-6, HF-10]; *hap2::HAP2-HA;MAR1-FLAG(−)*[CC-5284]; and *mar1;MAR1-FLAG;hap2;HAP2-HA(−)*[102,114,131]. Names denote strain origins and genotype; lowercase italics indicates the presence of a mutant gene, uppercase italics indicates the presence of the wild-type gene, double colons (::) indicate strains where transgene introduction was done through direct transformation by electroporation, and semi-colons (;) indicate the presence of a transgene introduced in this case, through genetic crosses of a previously-transformed parental strain and isolated in a progeny strain. Further details regarding the authentication and descriptions of the transgenic strains used in this study are provided in Figure S3 and Data S4.

Chlamydomonas transformation—*Chlamydomonas* cells were transformed by electroporation of plasmid DNA encoding the tagged *HAP2* or *MAR1* transgenes using a BioRad GenePulser Xcell (Shimogawara et al., 1998). *Spe*I-linearized *MAR1-FLAG* or *Sbf*I-linearized *HAP2-FLAG* plasmid DNA were transformed into *hap2(−)* and *mar1(−)* cells. The sequences of the plasmid DNAs used for transformation and of PCR products across the insertion site of the *mar1(−)* CLiP mutant, *LMJ.RY0402.185187,* were confirmed by analysis at the MGH CCIB DNA core and Eurofins, respectively. Positive transformants were selected for further analysis based on their growth on zeocin (10 μg/mL, Invitrogen) TAP-agar plates, presence of the *ble* gene product assessed by PCR of Chelex-100-extracted template DNA (Nouemssi et al., 2020) using primers Zeo_F1 and Zeo_R1, and immunoblotting of gamete lysates for expression of the FLAG-tagged proteins. Data S3 and S4 provide further details on plasmid construction, identification of transformants based on growth on selective media, PCR screening, and expression of tagged proteins.

Chlamydomonas crosses and progeny selection—For crosses (Figure S3), equal numbers of the indicated *plus* and *minus* gametes were mixed together and plated onto paromomycin (15 μg/mL, Sigma) TAP-agar plates at 0.5, 1, 1.5, and 2 h after mixing. Agar plates from crosses were exposed to continuous light for 16–24 h, then placed in the dark to allow zygote maturation. After at least 7 days in the dark, any remaining unfused cells were scraped towards the edges of the plate with a sterile razor blade and their further growth prevented by exposure of the plate to chloroform vapors for 30–60 sec. The thick cell walls of the zygospores remained attached to the agar and were resistant to the cytolytic effects of the chloroform vapors. After incubation under a 13:11 light-dark cycle at 21°C for 2 weeks to allow germination and visible colony growth, 20 – 30 colonies (each representing the vegetative haploid descendants of 4 initial meiotic progeny) were picked and resuspended

in N-free medium with shaking for 1 h to obtain a single-cell suspension, then re-plated onto TAP-agar plates to allow for growth of single colonies composed of individual meiotic progeny. Resulting colonies were screened for mating type, genotype and phenotype by PCR, western blotting, and behavior in mixing assays (Data S4) to isolate the desired genotypes.

METHOD DETAILS

Cell surface biotinylation—To prepare *hap2(−)* gametes for surface biotinylation, they were activated in db-cAMP buffer for 30 m (Sigma; Misamore *et al.*, 2003) before a 30 m incubation in 1 mg/mL Sulfo-NHS-LC-Biotin (ThermoFisher). Biotinylation was stopped by addition of 20 mM Tris (pH 7.3) followed by 3 washes in N-free medium. Activated, biotinylated *hap2(−)* gametes were mixed with an equal number of *FUS1-HA(+)* gametes, or, as a control, with *fus1(+)* gametes, for 30 m followed by lysis in 4 mL RIPA buffer (20 mM Tris, 150 mM NaCI, 1% NP-40, 0.5% DOC, 0.1% SDS and protease inhibitor cocktail, Wilson et al., 1999) and sonication 3 times (10 s each) on ice. The lysate was cleared by centrifugation for 30 m at 15,000 × g and incubated for 4 h at 4°C with anti-HA monoclonal antibody (Santa Cruz) and protein A sepharose (Sigma). The protein A sepharose was washed 4 × with 1/3 RIPA buffer (20 mM Tris, 150 mM NaCI, 0.33% NP-40, 0.17% DOC, 0.03% SDS with protease inhibitor cocktail) and eluted with 1 mg/mL HA peptide as described previously (Ning *et al.*, 2013), or by boiling in sample buffer. Biotinylated proteins in the eluate were detected on immunoblots using streptavidin-HRP (Jackson ImmunoResearch). The 250 kDa regions of similarly prepared samples were analyzed by mass spectrometry at the Proteomics Core at UT Southwestern Medical Center (Dallas, TX), identifying Cre03.g176961 peptides with 21.8% coverage of the MAR1 sequence (Data S2).

SDS-PAGE and Immunoblotting—For gamete lysates, 2.5×10^7 gametes were suspended in 225 μL N-free medium, and lysed by adding 75 μL of 4x SDS-PAGE sample buffer (1× concentration in sample = 40 mM Tris, pH 6.8, 1% SDS, 5% glycerol, 0.0003% Bromophenol blue, 1 mM EDTA and either 100 mM DTT or 5 mM TCEP) at 95°C for 5 −10 m. 2.5×10^6 cell equivalents were subjected to electrophoresis on SDS polyacrylamide tris-glycine gels (7 or 8%), transferred to PVDF membranes, blocked in 5% milk + TBSt buffer, and probed with either rat anti-HA (1/1000; Sigma, 3F10) or mouse anti-FLAG (1/5000, Sigma, M2) primary antibodies, followed by goat-anti-rat HRP or goat-anti-mouse HRP (1/5000; Millipore) secondary antibodies diluted in 0.5% milk + TBSt buffer. Tubulin was used as a loading control and was detected by probing with mouse anti-α-tubulin primary antibodies (1/5000; Sigma, B512). Immunoblots were developed with SuperSignal West Femto (Thermo Scientific) and exposed to film or scanned with a C-digit blot scanner (LI-COR). Images were processed using Image Studio software (LI-COR) and Adobe Illustrator and Photoshop.

Protease treatments—Protease treatments were performed as described previously (Liu *et al.*, 2010) with minor modifications. To assess surface localization of HAP2-HA and HAP2-FLAG, live *minus* gametes were treated with 0.05% trypsin for 20 m followed by 3 washes in N-free media with 0.1 mg/mL Trypsin inhibitor from chicken egg white (Sigma) before lysis in SDS-PAGE sample buffer. Surface localization of MAR1-FLAG

and HAP2-HA was also assessed by treating live gametes with 1% pronase (1.0 mg/mL, Sigma) for 20 m followed by 3 washes in N-free media with 1 mM PMSF before lysis in SDS-PAGE sample buffer.

Immunoprecipitations—For protein association assays, lysates were prepared from the indicated strains after gamete activation by mixing gametes for 30 – 60 m with fusion-defective *fus1(+)* or *hap2(−)* gametes. The mixed gametes were disrupted by lysis in cold detergent buffers supplemented with protease inhibitor cocktail (Roche); RIPA or 1% Triton X-100 (20 mM Tris, 150 mM NaCI, 1% Triton X-100) as indicated, then lysates were cleared by centrifugation for 30 m at 15,000 × g. Detergent supernatants were incubated rotating for 4 h at 4°C with protein A agarose or sepharose and a 1/100 dilution of anti-FLAG (Sigma, mouse M2 monoclonal or rabbit polyclonal) or anti-HA (Santa Cruz, mouse F-7 monoclonal or AbClonal, rabbit polyclonal) antibodies. The immunoprecipitates were either boiled directly in sample buffer or eluted with FLAG peptide (Sigma, 200 μg/mL) or HA peptide (Roche, 1 mg/mL). The presence of the tagged forms of FUS1, HAP2 and MAR1 proteins in *minus* gamete lysate input samples and immunoprecipitation eluates was assessed by SDS-PAGE followed by immunoblotting.

Recombinant protein production and interaction assays—For recombinant protein production, the expression vectors GST-rFUS1 and HIS-rMAR1 plasmids were transformed into BL21(DE3) (New England Biolabs) competent *E. coli* cells. Bacterial cells expressing the recombinant proteins were grown with shaking overnight at 37°C in liquid LB media containing antibiotics and then 0.5 mL was inoculated into 50 mL LB cultures. The cultures were shaken for 1 hour at 37°C and induced with IPTG (1 mM) for 3 h at 30°C. Bacteria were lysed in 0.9 mL lysis buffer (20 mM Tris pH 8.0, 150 mM NaCI, 5 mM DTT, 1 mg/mL lysozyme, 5 μg/mL DNase I, 10 μg/mL RNase A, and protease inhibitor cocktail) on ice for 30 m. Triton X-100 was added to 1% (final concentration), then samples were sonicated on ice for 1 m, cleared by centrifugation at 4°C 15,000 × g for 30 m and used in GST pull-down assays. *BL21/pGST-FUS1* supernatants were incubated with glutathione beads for 1 hour and washed 3× with washing buffer (20 mM Tris, 150 mM NaCI, 0.3% Triton X-100, protease inhibitor cocktail). The glutathione beads with bound GST-FUS1 were incubated with *BL21/pHis-MAR1* lysate overnight at 4°C, washed 3× with washing buffer, and incubated with elution buffer (50 mM Tris pH 8.0, 20 mM reduced glutathione, 0.3% Triton X-100, protease inhibitor cocktail). Recombinant GST protein was used as a control for the recombinant protein interaction assays.

MAR1 polyclonal antibody generation—Antibodies against MAR1 peptides (1 = TQPPRPPWPPRPPPAPPPS, residues 164–182; and 2 = QIPQAPRWPYPQLPSWPPAS, residues 214–233) were generated in rabbits by YenZym Antibodies (Brisbane, CA). Only polyclonal antibodies generated against peptide 1 were used. Antibodies were purified on peptide-conjugated affinity columns and specificity verified by immunoblotting with recombinant protein samples with and without MAR1 (Data S3).

Indirect immunofluorescence microscopy—Immunofluorescent staining of gametes was performed as described previously (Belzile *et al.*, 2013; Feng *et al.*, 2018; Ranjan *et al.*,

2019) with some modifications. Immunofluorescent staining of gametes was performed on samples of approximately 1×10^7 live gametes in N-free medium that were allowed to settle and adhere for 10–30 m on 0.1% poly-L-lysine coated slides or coverslips. Excess media and non-adhered cells were gently removed by pipetting before samples were plunged into ice-cold methanol for 20 m. In some cases, cells were pre-fixed with 4% paraformaldehyde for 10 m prior to methanol fixation to better preserve cilia (Ranjan *et al.*, 2019). For single staining with anti-HA antibodies (1/100, Sigma, 3F10) or anti-FLAG antibodies (1/100, Sigma, M2), gametes were blocked for 30 – 60 m in diluted goat serum (5% goat serum, 0.1% BSA, 0.5% Triton X-100, 1% cold-water fish gelatin in PBS). For double staining with anti-HA (1/100, Roche, 3F10) and anti-FLAG antibodies (1/100, Sigma, M2), gametes were blocked in diluted goat and donkey serum (5% donkey serum, 10% goat serum, 0.1% BSA, 0.5% Triton X-100, 1% cold-water fish gelatin in PBS). Primary antibodies were diluted in blocking sera and incubated with samples for 2 h at 20°C or overnight at 4°C, washed 3× with PBSt (PBS + 0.5% Triton X-100), and incubated with blocking-sera-diluted secondary antibodies for 2 h at 20°C. For anti-HA staining, the secondary antibody used was Alexa Fluor 488-conjugated goat anti-rat IgG (1/400, Invitrogen). For anti-FLAG staining, the secondary antibody used was Alexa Fluor 594-conjugated goat anti-mouse IgG (1/400, Invitrogen). Samples were washed 3× with PBSt and coverslips were mounted using either Fluoromount-G (Southern Biotech) or Prolong Gold antifade reagent (Invitrogen) and sealed with nail polish. Immunofluorescence images of gametes were captured on a Leica SP5 X Laser Scanning confocal microscope with a Leica 63x/1.4 NA oil objective lens. Images are individual z-sections or z-stack composites as indicated in the figure legends and were processed with Adobe photoshop and Leica LASAF software.

Differential interference contrast microscopy—Ciliary adhesion between *minus* and *plus* gametes was assessed by differential interference contrast (DIC) microscopy using an inverted Axiovert 135 TV microscope fitted with an ORCA-ER (Hamamatsu) digital camera and a 5x/0.15 NA DIC Epiplan NEOFLUAR objective lens controlled by StreamPix software (NorPix). Scale bars were drawn based on similarly acquired image taken of the known grid lengths of an Improved Neubauer hemocytometer slide.

Scanning electron microscopy—For examination of ciliary adhesion by scanning electron microscopy, WT*(+)* gametes were mixed with *mar1;hap2(−)* gametes for 30 m, washed 10x in sterile-filtered N-free media, fixed for 20 m in Parducz fixative (1 part saturated $HgCl_2$, 6 parts 2%OsO_4)(Parducz, 1967), then aliquots of the cells suspended in fixative were transferred onto 0.1% poly-L-lysine coated coverslips for an additional 45 m. Coverslips were washed 10× in ddH2O, then dehydrated by sequential washes (3× each, 2 m/wash) in 70%, 95%, and 100% ethanol solutions. Coverslips were critical point dried from CO_2 and mounted on stubs over double-sided tape before being sputter-coated with gold–palladium (60%:40%) (Balzers Med 010) and observed using a scanning electron microscope (Hitachi S-4700 FESEM) at an accelerating voltage of 5 kV in high vacuum.

Chlamydomonas bioassays—Assays used to quantify gamete activation, mating structure adhesion and cell-cell fusion were performed as previously described (Feng *et al.*, 2018) with minor modifications. Gamete activation was assayed by cell wall loss, as

quantified by the amount of OD435-detectable chlorophyll released into the supernatant upon treatment of mixed gametes with a detergent buffer (Feng *et al.*, 2018; Snell, 1982; Wang et al., 2006). Equal numbers of *plus* and *minus* gametes of the indicated genotypes were mixed for 10 m at a concentration of 5×10^7 cells/mL before being added to 1.6 volumes of 4°C N-free medium containing 0.075% Triton-X 100 and 5mM EDTA (pH8), vortexed, centrifuged at 8700 × g for 30 s, and $OD435_{exp}$ of supernatant determined by a Nanodrop 2000 spectrophotometer. The maximum $OD435_{max}$ (representing 100% cell wall loss) for individual samples was then obtained after resuspending and sonicating samples for 12 s with a Microson XL sonicator. Percent cell wall loss was calculated as: $[(OD435_{max} - OD435_{exp})/ OD435_{max}] \times 100$. Mating structure adhesion was assayed in *plus* and *minus* gametes mixed in equal numbers at a concentration of 5.0×10^7cells/mL for 10 m, followed by fixation in an equal volume of 5% glutaraldehyde (Feng *et al.*, 2018). Ciliary adhesions were disrupted by pipetting 20× with a 200 μL pipette tip. Glutaraldehyde fixation coupled with the light agitation from pipetting disrupts flagellar adhesions leaving pairs of *plus* and *minus* gametes attached only by their mating structures (Feng *et al.*, 2018; Forest, 1983). The percent of gametes attached by their mating structures was calculated as: [(2 × number of pairs) / (2 × number of pairs + number of single gametes)] × 100. Gamete fusion was assayed by the microscopic enumeration of quadri-ciliated cells from equal numbers of *plus* and *minus* gametes mixed for 10 m and fixed in an equal volume of 5% glutaraldehyde as previously described (Feng *et al.*, 2018). The percent of gamete fusion was calculated as: [(2 × number of quadri-ciliated cells) / (2 × number of quadri-ciliated cells + number of single gametes)] × 100. For assessment of gamete activation, 4 independent cell wall loss experiments were performed for each cross tested. For adhesion and fusion experiments, at least 200 cells (as either singles or pairs) were counted in each of at least 5 biological replicates per cross. Gamete strains used for quantification of gamete activation, mating structure adhesion, and gamete fusion were the F_1 and F_2 progeny strains derived from crosses of the original *mar1(−)* CLiP mutant strain *LMJ.RY0402.185187,* which had been transformed with the MAR1-FLAG encoding transgene (Figure S3 and Data S3 and S4). Preliminary results gathered using the *LMJ.RY0402.185187(−)* gametes agreed with the phenotypes observed in the *mar1(−)* progeny strains.

Sequence homology detection and protein structure modeling—The similarity of the ectodomain sequence of *Chlamydomonas reinhardtii* FUS1 (GenBank#:AAC49416, residues 18–791) to plant GEX2 species was detected by DELTA-BLAST (Boratyn et al., 2012) and PSI-BLAST (Altschul et al., 1997; Aravind and Koonin, 1999), with significant hits to GEX2 family members detected upon iterative searches (Table S1). The online tool PROMALS3D (Pei and Grishin, 2007) was used to construct the FUS1 and GEX2 ectodomain sequence alignment shown in Data S1. The RaptorX Structure Prediction web server hosting the CASP12 and CASP13 top-ranked contact prediction method for modeling protein structure from a given amino acid sequence irrespective of coevolution information (Källberg et al., 2012; Xu, 2019; Xu *et al.*, 2021) was used to construct structural models of the *C. reinhardtii* FUS1 and *A. thaliana* GEX2 ectodomains and to identify previously undetected Ig-like domains. Images of the FUS1 and GEX2 structural models (Fig. 1B) were generated using PyMol software (Schrodinger, LLC). Structural homologies of GEX2, FUS1 and MAR1 (GenBank: KT288268) with existing structures in the Protein Data Bank

were detected using the RaptorX template-based structural modeling server (Källberg *et al.*, 2012), PHYRE2 (Kelley et al., 2015), SWISS-MODEL (Waterhouse et al., 2018) and HHPRED (Zimmermann et al., 2018).

QUANTIFICATION AND STATISTICAL ANALYSIS

Quantification of HAP2 signals—Surface and total tagged HAP2 protein signals on digital images of immunoblots were quantified using Image Studio Digits software (LI-COR) and tubulin was used for normalization. For quantification of relative protein abundance median signal intensities were determined within rectangles drawn around the upper, surface band of HAP2, the lower, internal band of HAP2, and α-tubulin on digital images of immunoblots. Background correction was performed by ImageStudioDigits software (LI-COR) using a right/left border setting of 2 on each rectangle. Total HAP2 signal was calculated as the sum of the signals of the upper and lower HAP2 bands. To compare total HAP2 proportions respective to tubulin loading controls across multiple blots, lane normalization factors were calculated for both total HAP2 and α-tubulin as described by the vendor (LI-COR). The percentage of surface-expressed HAP2 for each sample was calculated as [(signal of HAP2 upper band)/(Total HAP2 signal)] ×100. For quantification of HAP2-HA immunofluorescence signals, system-optimized z-sections of immunostained *mar1;HAP2-HA(−)*, *hap2;HAP2-HA(−)*, and *hap2(−)* naive gametes were acquired by the Leica SP5 X Laser Scanning confocal microscope using equivalent gain, laser, and zoom factor settings. Max projection images were created of the z-sections using Leica LAS X core module software and the lasso tool was used to draw a region of interest (ROI) around each cell in a given field of view and record its mean value intensity within the Ax488 channel. HAP2-HA signals of individual cells from nine fields of view were measured for the *mar1;HAP2-HA(−)*, *hap2;HAP2-HA(−)* samples, and six fields of view were measured for *hap2(−)* samples.

Statistical Analyses—Data were analyzed using Prism 9.0 software (GraphPad) and are presented as median or mean ± SD with or without raw data points for individual biological replicates as indicated in the figure legends. Significance was defined as a p-value <0.05. In part to determine whether data met assumptions of the statistical approach (for parametric vs. non-parametric tests), data from experimental groups were first subjected to Shapiro-Wilk, D'Agostino & Pearson and Kolmogorov-Smirnov normality tests. The statistical tests used to analyze data from each experiment, what n represents, and the exact value of n are indicated in the figure legends.

Supplementary Material

Refer to Web version on PubMed Central for supplementary material.

Acknowledgments

We thank UMD colleagues Jocelyn Chen and Drs. Jun Zhang, Mayanka Awasthi, and Peeyush Ranjan; UT Southwestern colleagues Drs. Muqing Cao, Wenhao Li, Jue Ning, and Saikat Mukhopadhyay; Institut Pasteur colleagues Drs. Felix Rey, Eduard Salazar, and Ignacio Fernandez; and colleague, Ursula Goodenough, Washington University, St. Louis, for helpful discussions; Dr. Tim Maugel of the UMD Laboratory for Biological Ultrastructure for assistance with SEM; and Drs. Kate Luby-Phelps and Abhijit Bugde (UT Southwestern Medical Center, Live

Cell Imaging Core) and Amy Beaven (UMD, Imaging Core) for guidance with light microscopy. Funding was provided by NIH GM56778 and GM122565 to W.J.S. and F32-GM126735 to J.F.P.

References

Altschul SF, Madden TL, Schaffer AA, Zhang J, Zhang Z, Miller W, and Lipman DJ (1997). Gapped BLAST and PSI-BLAST: a new generation of protein database search programs. Nucleic Acids Res. 25, 3389–3402. 10.1093/nar/25.17.3389. [PubMed: 9254694]

Andersson H, Barth BU, Ekström M, and Garoff H (1997). Oligomerization-dependent folding of the membrane fusion protein of Semliki Forest virus. J. Virol. 71, 9654–9663. [PubMed: 9371630]

Aravind L, and Koonin EV (1999). Gleaning non-trivial structural, functional and evolutionary information about proteins by iterative database searches. J. Mol. Biol. 287, 1023–1040. 10.1006/jmbi.1999.2653. [PubMed: 10222208]

Aydin H, Sultana A, Li S, Thavalingam A, and Lee JE (2016). Molecular architecture of the human sperm IZUMO1 and egg JUNO fertilization complex. Nature 534, 562–565. 10.1038/nature18595. [PubMed: 27309818]

Baquero E, Fedry J, Legrand P, Krey T, and Rey FA (2019). Species-Specific Functional Regions of the Green Alga Gamete Fusion Protein HAP2 Revealed by Structural Studies. Structure 27, 113–124 e114. 10.1016/j.str.2018.09.014. [PubMed: 30416037]

Barbaux S, Ialy-Radio C, Chalbi M, Dybal E, Homps-Legrand M, Do Cruzeiro M, Vaiman D, Wolf J-P, and Ziyyat A (2020). Sperm SPACA6 protein is required for mammalian Sperm-Egg Adhesion/Fusion. Sci. Rep 10, 1–15. 10.1038/s41598-020-62091-y. [PubMed: 31913322]

Beh CT, Brizzio V, and Rose MD (1997). KAR5 encodes a novel pheromone-inducible protein required for homotypic nuclear fusion. J. Cell Biol. 139, 1063–1076. 10.1083/jcb.139.5.1063. [PubMed: 9382856]

Belzile O, Hernandez-Lara CI, Wang Q, and Snell WJ (2013). Regulated membrane protein entry into flagella is facilitated by cytoplasmic microtubules and does not require IFT. Curr. Biol. 23, 1460–1465. 10.1016/j.cub.2013.06.025. [PubMed: 23891117]

Bianchi E, Doe B, Goulding D, and Wright GJ (2014). Juno is the egg Izumo receptor and is essential for mammalian fertilization. Nature 508, 483–487. 10.1038/nature13203. [PubMed: 24739963]

Bianchi E, and Wright GJ (2020). Find and fuse: Unsolved mysteries in sperm–egg recognition. PLoS Biol. 18, e3000953. 10.1371/journal.pbio.3000953. [PubMed: 33186358]

Blom N, Sicheritz-Pontén T, Gupta R, Gammeltoft S, and Brunak S (2004). Prediction of post-translational glycosylation and phosphorylation of proteins from the amino acid sequence. Proteomics 4, 1633–1649. 10.1002/pmic.200300771. [PubMed: 15174133]

Boratyn GM, Schäffer AA, Agarwala R, Altschul SF, Lipman DJ, and Madden TL (2012). Domain enhanced lookup time accelerated BLAST. Biol Direct 7, 12. 10.1186/1745-6150-7-12. [PubMed: 22510480]

Camacho-Nuez M, Hernandez-Silva DJ, Castaneda-Ortiz EJ, Paredes-Martinez ME, Rocha-Martinez MK, Alvarez-Sanchez ME, Mercado-Curiel RF, Aguilar-Tipacamu G, and Mosqueda J (2017). Hap2, a novel gene in *Babesia bigemina* is expressed in tick stages, and specific antibodies block zygote formation. Parasit Vectors 10, 568. 10.1186/s13071-017-2510-0. [PubMed: 29132437]

Carleton M, Lee H, Mulvey M, and Brown DT (1997). Role of glycoprotein PE2 in formation and maturation of the Sindbis virus spike. J. Virol. 71, 1558–1566. [PubMed: 8995682]

Cervantes MD, Hamilton EP, Xiong J, Lawson MJ, Yuan D, Hadjithomas M, Miao W, and Orias E (2013). Selecting one of several mating types through gene segment joining and deletion in *Tetrahymena thermophila*. PLoS Biol. 11, e1001518. 10.1371/journal.pbio.1001518. [PubMed: 23555191]

Chatterjee S, Basak AJ, Nair AV, Duraivelan K, and Samanta D (2020). Immunoglobulin-fold containing bacterial adhesins: molecular and structural perspectives in host tissue colonization and infection. FEMS Microbiol. Lett. 368, fnaa220. 10.1093/femsle/fnaa220.

Cole ES, Cassidy-Hanley D, Fricke Pinello J, Zeng H, Hsueh M, Kolbin D, Ozzello C, Giddings T Jr., Winey M, and Clark TG (2014). Function of the male-gamete-specific fusion protein HAP2 in a seven-sexed ciliate. Curr. Biol. 24, 2168–2173. 10.1016/j.cub.2014.07.064. [PubMed: 25155508]

Cyprys P, Lindemeier M, and Sprunck S (2019). Gamete fusion is facilitated by two sperm cell-expressed DUF679 membrane proteins. Nature Plants 5, 253–257. [PubMed: 30850817]

Dean J (2007). The enigma of sperm-egg recognition in mice. Soc Reprod Fertil Suppl 63, 359–365. [PubMed: 17566284]

Dresselhaus T, Sprunck S, and Wessel GM (2016). Fertilization Mechanisms in Flowering Plants. Curr. Biol. 26, R125–139. 10.1016/j.cub.2015.12.032. [PubMed: 26859271]

Ebchuqin E, Yokota N, Yamada L, Yasuoka Y, Akasaka M, Arakawa M, Deguchi R, Mori T, and Sawada H (2014). Evidence for participation of GCS1 in fertilization of the starlet sea anemone *Nematostella vectensis*: implication of a common mechanism of sperm-egg fusion in plants and animals. Biochem. Biophys. Res. Commun. 451, 522–528. 10.1016/j.bbrc.2014.08.006. [PubMed: 25111819]

Engel ML, Holmes-Davis R, and McCormick S (2005). Green sperm. Identification of male gamete promoters in *Arabidopsis*. Plant Physiol. 138, 2124–2133. 10.1104/pp.104.054213. [PubMed: 16055690]

Fedry J, Forcina J, Legrand P, Pehau-Arnaudet G, Haouz A, Johnson M, Rey FA, and Krey T (2018). Evolutionary diversification of the HAP2 membrane insertion motifs to drive gamete fusion across eukaryotes. PLoS Biol. 16, e2006357. 10.1371/journal.pbio.2006357. [PubMed: 30102690]

Fedry J, Liu Y, Pehau-Arnaudet G, Pei J, Li W, Tortorici MA, Traincard F, Meola A, Bricogne G, Grishin NV, et al. (2017). The Ancient Gamete Fusogen HAP2 Is a Eukaryotic Class II Fusion Protein. Cell 168, 904–915 e910. 10.1016/j.cell.2017.01.024. [PubMed: 28235200]

Feng J, Dong X, Pinello J, Zhang J, Lu C, Iacob RE, Engen JR, Snell WJ, and Springer TA (2018). Fusion surface structure, function, and dynamics of gamete fusogen HAP2. Elife 7, e39772. 10.7554/eLife.39772. [PubMed: 30281023]

Ferris PJ, Pavlovic C, Fabry S, and Goodenough UW (1997). Rapid evolution of sex-related genes in *Chlamydomonas*. Proc. Natl. Acad. Sci. USA 94, 8634–8639. 10.1073/pnas.94.16.8634. [PubMed: 9238029]

Ferris PJ, Waffenschmidt S, Umen JG, Lin H, Lee JH, Ishida K, Kubo T, Lau J, and Goodenough UW (2005). Plus and minus sexual agglutinins from *Chlamydomonas reinhardtii*. Plant Cell 17, 597–615. 10.1105/tpc.104.028035. [PubMed: 15659633]

Ferris PJ, Woessner JP, and Goodenough UW (1996). A sex recognition glycoprotein is encoded by the plus mating-type gene fus1 of *Chlamydomonas reinhardtii*. Mol. Biol. Cell 7, 1235–1248. [PubMed: 8856667]

Ferris PJ, Woessner JP, Waffenschmidt S, Kilz S, Drees J, and Goodenough UW (2001). Glycosylated polyproline II rods with kinks as a structural motif in plant hydroxyproline-rich glycoproteins. Biochemistry 40, 2978–2987. 10.1021/bi0023605. [PubMed: 11258910]

Fischer N, and Rochaix JD (2001). The flanking regions of PsaD drive efficient gene expression in the nucleus of the green alga *Chlamydomonas reinhardtii*. Mol. Genet. Genomics 265, 888–894. 10.1007/s004380100485. [PubMed: 11523806]

Forest CL (1983). Specific contact between mating structure membranes observed in conditional fusion-defective *Chlamydomonas* mutants. Exp. Cell Res. 148, 143–154. 10.1016/0014-4827(83)90194-5. [PubMed: 6628554]

Friedmann I, Colwin AL, and Colwin LH (1968). Fine-structural aspects of fertilization in *Chlamydomonas reinhardi*. J. Cell Sci. 3, 115–128. [PubMed: 5641603]

Fujihara Y, Lu YG, Noda T, Oji A, Larasati T, Kojima-Kita K, Yu ZF, Matzuk RM, Matzuk MM, and Ikawa M (2020). Spermatozoa lacking Fertilization Influencing Membrane Protein (FIMP) fail to fuse with oocytes in mice. Proc. Natl. Acad. Sci. USA 117, 9393–9400. 10.1073/pnas.1917060117. [PubMed: 32295885]

Goodstein DM, Shu S, Howson R, Neupane R, Hayes RD, Fazo J, Mitros T, Dirks W, Hellsten U, Putnam N, and Rokhsar DS (2012). Phytozome: a comparative platform for green plant genomics. Nucleic Acids Res. 40, D1178–1186. 10.1093/nar/gkr944. [PubMed: 22110026]

Grayson P (2015). Izumo1 and Juno: the evolutionary origins and coevolution of essential sperm-egg binding partners. R. Soc. Open Sci. 2, 150296. ARTN 150296 10.1098/rsos.150296. [PubMed: 27019721]

Hamburger ZA, Brown MS, Isberg RR, and Bjorkman PJ (1999). Crystal structure of invasin: A bacterial integrin-binding protein. Science 286, 291–295. DOI 10.1126/science.286.5438.291. [PubMed: 10514372]

Heiman MG, and Walter P (2000). Prm1p, a pheromone-regulated multispanning membrane protein, facilitates plasma membrane fusion during yeast mating. J. Cell Biol. 151, 719–730. 10.1083/jcb.151.3.719. [PubMed: 11062271]

Herberg S, Gert KR, Schleiffer A, and Pauli A (2018). The Ly6/uPAR protein Bouncer is necessary and sufficient for species-specific fertilization. Science 361, 1029–1033. 10.1126/science.aat7113. [PubMed: 30190407]

Hirai M, Arai M, Mori T, Miyagishima SY, Kawai S, Kita K, Kuroiwa T, Terenius O, and Matsuoka H (2008). Male fertility of malaria parasites is determined by GCS1, a plant-type reproduction factor. Curr. Biol. 18, 607–613. 10.1016/j.cub.2008.03.045. [PubMed: 18403203]

Honig B, and Shapiro L (2020). Adhesion Protein Structure, Molecular Affinities, and Principles of Cell-Cell Recognition. Cell 181, 520–535. 10.1016/j.cell.2020.04.010. [PubMed: 32359436]

Ikawa M, Inoue N, Benham AM, and Okabe M (2010). Fertilization: a sperm's journey to and interaction with the oocyte. J. Clin. Invest. 120, 984–994. 10.1172/JCI41585. [PubMed: 20364096]

Inoue N, Ikawa M, Isotani A, and Okabe M (2005). The immunoglobulin superfamily protein Izumo is required for sperm to fuse with eggs. Nature 434, 234–238. 10.1038/nature03362. [PubMed: 15759005]

Johnson MA, von Besser K, Zhou Q, Smith E, Aux G, Patton D, Levin JZ, and Preuss D (2004). *Arabidopsis* hapless mutations define essential gametophytic functions. Genetics 168, 971–982. 10.1534/genetics.104.029447. [PubMed: 15514068]

Jones DT (1999). Protein secondary structure prediction based on position-specific scoring matrices. J. Mol. Biol. 292, 195–202. 10.1006/jmbi.1999.3091. [PubMed: 10493868]

Kadandale P, Stewart-Michaelis A, Gordon S, Rubin J, Klancer R, Schweinsberg P, Grant BD, and Singson A (2005). The egg surface LDL receptor repeat-containing proteins EGG-1 and EGG-2 are required for fertilization in *Caenorhabditis elegans*. Curr. Biol. 15, 2222–2229. 10.1016/j.cub.2005.10.043. [PubMed: 16360684]

Käll L, Krogh A, and Sonnhammer ELL (2007). Advantages of combined transmembrane topology and signal peptide prediction--the Phobius web server. Nucleic Acids Res. 35, W429–432. 10.1093/nar/gkm256. [PubMed: 17483518]

Källberg M, Wang H, Wang S, Peng J, Wang Z, Lu H, and Xu J (2012). Template-based protein structure modeling using the RaptorX web server. Nat. Protoc. 7, 1511–1522. 10.1038/nprot.2012.085. [PubMed: 22814390]

Kelley LA, Mezulis S, Yates CM, Wass MN, and Sternberg MJE (2015). The Phyre2 web portal for protein modeling, prediction and analysis. Nat. Protoc. 10, 845–858. 10.1038/nprot.2015.053. [PubMed: 25950237]

Lamas-Toranzo I, Hamze JG, Bianchi E, Fernandez-Fuertes B, Perez-Cerezales S, Laguna-Barraza R, Fernandez-Gonzalez R, Lonergan P, Gutierrez-Adan A, Wright GJ, et al. (2020). TMEM95 is a sperm membrane protein essential for mammalian fertilization. Elife 9, e53913. ARTN e53913 10.7554/eLife.53913. [PubMed: 32484434]

Le Naour F, Rubinstein E, Jasmin C, Prenant M, and Boucheix C (2000). Severely reduced female fertility in CD9-deficient mice. Science 287, 319–321. 10.1126/science.287.5451.319. [PubMed: 10634790]

Li X, Patena W, Fauser F, Jinkerson RE, Saroussi S, Meyer MT, Ivanova N, Robertson JM, Yue R, Zhang R, et al. (2019). A genome-wide algal mutant library and functional screen identifies genes required for eukaryotic photosynthesis. Nat. Genet. 51, 627–635. 10.1038/s41588-019-0370-6. [PubMed: 30886426]

Lillie FR (1914). Studies of fertilization. VI. The mechanism of fertilization in *Arbacia*. J. Exp. Zool. 16, 523–590. 10.1002/jez.1400160404.

Lin H, Guo S, and Dutcher SK (2018). RPGRIP1L helps to establish the ciliary gate for entry of proteins. J. Cell Sci. 131. 10.1242/jcs.220905.

Lin HW, Miller ML, Granas DM, and Dutcher SK (2013). Whole Genome Sequencing Identifies a Deletion in Protein Phosphatase 2A That Affects Its Stability and Localization in *Chlamydomonas reinhardtii*. PLoS Genet 9. ARTN e1003841 10.1371/journal.pgen.1003841.

Liu Y, Misamore MJ, and Snell WJ (2010). Membrane fusion triggers rapid degradation of two gamete-specific, fusion-essential proteins in a membrane block to polygamy in *Chlamydomonas*. Development 137, 1473–1481. 10.1242/dev.044743. [PubMed: 20335357]

Liu Y, Pei J, Grishin N, and Snell WJ (2015). The cytoplasmic domain of the gamete membrane fusion protein HAP2 targets the protein to the fusion site in *Chlamydomonas* and regulates the fusion reaction. Development 142, 962–971. 10.1242/dev.118844. [PubMed: 25655701]

Liu Y, Tewari R, Ning J, Blagborough AM, Garbom S, Pei J, Grishin NV, Steele RE, Sinden RE, Snell WJ, and Billker O (2008). The conserved plant sterility gene HAP2 functions after attachment of fusogenic membranes in *Chlamydomonas* and *Plasmodium* gametes. Genes Dev. 22, 1051–1068. 10.1101/gad.1656508. [PubMed: 18367645]

Lorenzetti D, Poirier C, Zhao M, Overbeek PA, Harrison W, and Bishop CE (2014). A transgenic insertion on mouse chromosome 17 inactivates a novel immunoglobulin superfamily gene potentially involved in sperm-egg fusion. Mamm. Genome 25, 141–148. 10.1007/s00335-013-9491-x. [PubMed: 24275887]

Misamore MJ, Gupta S, and Snell WJ (2003). The *Chlamydomonas* Fus1 protein is present on the mating type plus fusion organelle and required for a critical membrane adhesion event during fusion with minus gametes. Mol. Biol. Cell 14, 2530–2542. 10.1091/mbc.e02-12-0790. [PubMed: 12808049]

Miyado K, Yamada G, Yamada S, Hasuwa H, Nakamura Y, Ryu F, Suzuki K, Kosai K, Inoue K, Ogura A, et al. (2000). Requirement of CD9 on the egg plasma membrane for fertilization. Science 287, 321–324. 10.1126/science.287.5451.321. [PubMed: 10634791]

Mori T, Igawa T, Tamiya G, Miyagishima S-Y, and Berger F (2014). Gamete attachment requires GEX2 for successful fertilization in *Arabidopsis*. Curr. Biol. 24, 170–175. 10.1016/j.cub.2013.11.030. [PubMed: 24388850]

Mori T, Kuroiwa H, Higashiyama T, and Kuroiwa T (2006). GENERATIVE CELL SPECIFIC 1 is essential for angiosperm fertilization. Nat. Cell Biol. 8, 64–71. 10.1038/ncb1345. [PubMed: 16378100]

Navaratnarajah CK, Generous AR, Yousaf I, and Cattaneo R (2020). Receptor-mediated cell entry of paramyxoviruses: Mechanisms, and consequences for tropism and pathogenesis. J. Biol. Chem. 295, 2771–2786. 10.1074/jbc.REV119.009961. [PubMed: 31949044]

Necci M, Piovesan D, Dosztányi Z, and Tosatto SCE (2017). MobiDB-lite: fast and highly specific consensus prediction of intrinsic disorder in proteins. Bioinformatics 33, 1402–1404. 10.1093/bioinformatics/btx015. [PubMed: 28453683]

Nielsen H (2017). Predicting Secretory Proteins with SignalP. Methods in Molecular Biology (Clifton, N.J.) 1611, 59–73. 10.1007/978-1-4939-7015-5_6.

Ning J, Otto TD, Pfander C, Schwach F, Brochet M, Bushell E, Goulding D, Sanders M, Lefebvre PA, Pei J, et al. (2013). Comparative genomics in *Chlamydomonas* and *Plasmodium* identifies an ancient nuclear envelope protein family essential for sexual reproduction in protists, fungi, plants, and vertebrates. Genes Dev. 27, 1198–1215. 10.1101/gad.212746.112. [PubMed: 23699412]

Nishimura H, and L'Hernault SW (2016). Gamete interactions require transmembranous immunoglobulin-like proteins with conserved roles during evolution. Worm 5, e1197485. 10.1080/21624054.2016.1197485. [PubMed: 27695654]

Nishimura H, Tajima T, Comstra HS, Gleason EJ, and L'Hernault SW (2015). The Immunoglobulin-like Gene spe-45 Acts during Fertilization in *Caenorhabditis elegans* like the Mouse Izumo1 Gene. Curr. Biol. 25, 3225–3231. 10.1016/j.cub.2015.10.056. [PubMed: 26671669]

Noda T, Lu YG, Fujihara Y, Oura S, Koyano T, Kobayashi S, Matzuk MM, and Ikawa M (2020). Sperm proteins SOF1, TMEM95, and SPACA6 are required for sperm-oocyte fusion in mice. Proc. Natl. Acad. Sci. USA 117, 11493–11502. 10.1073/pnas.1922650117. [PubMed: 32393636]

Nouemssi SB, Ghribi M, Beauchemin R, Meddeb-Mouelhi F, Germain H, and Desgagne-Penix I (2020). Rapid and Efficient Colony-PCR for High Throughput Screening of Genetically Transformed *Chlamydomonas reinhardtii*. Life 10, 186. 10.3390/life10090186.

Ohto U, Ishida H, Krayukhina E, Uchiyama S, Inoue N, and Shimizu T (2016). Structure of IZUMO1-JUNO reveals sperm-oocyte recognition during mammalian fertilization. Nature 534, 566–569. 10.1038/nature18596. [PubMed: 27309808]

Okamoto M, Yamada L, Fujisaki Y, Bloomfield G, Yoshida K, Kuwayama H, Sawada H, Mori T, and Urushihara H (2016). Two HAP2-GCS1 homologs responsible for gamete interactions in the cellular slime mold with multiple mating types: Implication for common mechanisms of sexual reproduction shared by plants and protozoa and for male-female differentiation. Dev. Biol. 415, 6–13. 10.1016/j.ydbio.2016.05.018. [PubMed: 27189178]

Pagni M, Ioannidis V, Cerutti L, Zahn-Zabal M, Jongeneel CV, Hau J, Martin O, Kuznetsov D, and Falquet L (2007). MyHits: improvements to an interactive resource for analyzing protein sequences. Nucleic Acids Res. 35, W433–437. 10.1093/nar/gkm352. [PubMed: 17545200]

Parducz B (1967). Ciliary movement and coordination in ciliates. Int. Rev. Cytol. 21, 91–128. 10.1016/s0074-7696(08)60812-8. [PubMed: 4961084]

Pei J, and Grishin NV (2007). PROMALS: towards accurate multiple sequence alignments of distantly related proteins. Bioinformatics 23, 802–808. 10.1093/bioinformatics/btm017. [PubMed: 17267437]

Perez-Vargas J, Krey T, Valansi C, Avinoam O, Haouz A, Jamin M, Raveh-Barak H, Podbilewicz B, and Rey FA (2014). Structural basis of eukaryotic cell-cell fusion. Cell 157, 407–419. 10.1016/j.cell.2014.02.020. [PubMed: 24725407]

Pinello JF, Lai AL, Millet JK, Cassidy-Hanley D, Freed JH, and Clark TG (2017). Structure-Function Studies Link Class II Viral Fusogens with the Ancestral Gamete Fusion Protein HAP2. Curr. Biol. 27, 651–660. 10.1016/j.cub.2017.01.049. [PubMed: 28238660]

Proschold T, Harris EH, and Coleman AW (2005). Portrait of a species: *Chlamydomonas reinhardtii*. Genetics 170, 1601–1610. 10.1534/genetics.105.044503. [PubMed: 15956662]

Ramakrishnan C, Maier S, Walker RA, Rehrauer H, Joekel DE, Winiger RR, Basso WU, Grigg ME, Hehl AB, Deplazes P, and Smith NC (2019). An experimental genetically attenuated live vaccine to prevent transmission of *Toxoplasma gondii* by cats. Sci. Rep. 9, 1474. 10.1038/s41598-018-37671-8. [PubMed: 30728393]

Ranjan P, Awasthi M, and Snell WJ (2019). Transient Internalization and Microtubule-Dependent Trafficking of a Ciliary Signaling Receptor from the Plasma Membrane to the Cilium. Curr. Biol. 29, 2942–2947 e2942. 10.1016/j.cub.2019.07.022. [PubMed: 31422889]

Sager R (1955). Inheritance in the Green Alga *Chlamydomonas Reinhardi*. Genetics 40, 476–489. [PubMed: 17247567]

Sankaranarayanan S, and Higashiyama T (2018). Capacitation in Plant and Animal Fertilization. Trends Plant Sci. 23, 129–139. 10.1016/j.tplants.2017.10.006. [PubMed: 29170007]

Shimogawara K, Fujiwara S, Grossman A, and Usuda H (1998). High-efficiency transformation of *Chlamydomonas reinhardtii* by electroporation. Genetics 148, 1821–1828. [PubMed: 9560396]

Singaravelu G, Rahimi S, Krauchunas A, Rizvi A, Dharia S, Shakes D, Smith H, Golden A, and Singson A (2015). Forward Genetics Identifies a Requirement for the Izumo-like Immunoglobulin Superfamily spe-45 Gene in *Caenorhabditis elegans* Fertilization. Curr. Biol. 25, 3220–3224. 10.1016/j.cub.2015.10.055. [PubMed: 26671668]

Singson A, Mercer KB, and L'Hernault SW (1998). The *C. elegans* spe-9 gene encodes a sperm transmembrane protein that contains EGF-like repeats and is required for fertilization. Cell 93, 71–79. 10.1016/s0092-8674(00)81147-2. [PubMed: 9546393]

Snell WJ (1982). Study of the release of cell wall degrading enzymes during adhesion of *Chlamydomonas* gametes. Exp. Cell Res. 138, 109–119. 10.1016/0014-4827(82)90096-9. [PubMed: 6802661]

Snell WJ, and Goodenough UW (2009). Flagellar adhesion, flagellar-generated signaling, and gamete fusion during mating. In The *Chlamydomonas* Sourcebook, Witman GB, ed. (Elsevier), pp. 369–394.

Steele RE, and Dana CE (2009). Evolutionary history of the HAP2/GCS1 gene and sexual reproduction in metazoans. PLoS One 4, e7680. 10.1371/journal.pone.0007680. [PubMed: 19888453]

Swanson WJ, and Vacquier VD (2002). The rapid evolution of reproductive proteins. Nat. Rev. Genet. 3, 137–144. 10.1038/nrg733. [PubMed: 11836507]

Tajima T, and Nishimura H (2018). Immunoglobulin-Like Domains Have an Evolutionarily Conserved Role During Gamete Fusion in *C. elegans* and Mouse. In Origin and Evolution of Biodiversity, Pontarotti P, ed. (Springer International Publishing), pp. 163–179.

Takahashi T, Mori T, Ueda K, Yamada L, Nagahara S, Higashiyama T, Sawada H, and Igawa T (2018). The male gamete membrane protein DMP9/DAU2 is required for double fertilization in flowering plants. Development 145, dev170076. 10.1242/dev.170076. [PubMed: 30487178]

Valansi C, Moi D, Leikina E, Matveev E, Graña M, Chernomordik LV, Romero H, Aguilar PS, and Podbilewicz B (2017). *Arabidopsis* HAP2/GCS1 is a gamete fusion protein homologous to somatic and viral fusogens. J. Cell Biol. 216, 571–581. [PubMed: 28137780]

van Dijk MR, van Schaijk BC, Khan SM, van Dooren MW, Ramesar J, Kaczanowski S, van Gemert GJ, Kroeze H, Stunnenberg HG, Eling WM, et al. (2010). Three members of the 6-cys protein family of *Plasmodium* play a role in gamete fertility. PLoS Pathog 6, e1000853. 10.1371/journal.ppat.1000853. [PubMed: 20386715]

Wang Q, Pan J, and Snell WJ (2006). Intraflagellar Transport Particles Participate Directly in Cilium-Generated Signaling in *Chlamydomonas*. Cell 125, 549–562. 10.1016/j.cell.2006.02.044. [PubMed: 16678098]

Waterhouse A, Bertoni M, Bienert S, Studer G, Tauriello G, Gumienny R, Heer FT, de Beer TAP, Rempfer C, Bordoli L, et al. (2018). SWISS-MODEL: homology modelling of protein structures and complexes. Nucleic Acids Res. 46, W296–W303. 10.1093/nar/gky427. [PubMed: 29788355]

Weiss RL, Goodenough DA, and Goodenough UW (1977). Membrane differentiations at sites specialized for cell fusion. J. Cell Biol. 72, 144–160. [PubMed: 830653]

Wilson NF, O'Connell JS, Lu M, and Snell WJ (1999). Flagellar adhesion between mt(+) and mt(−) *Chlamydomonas* gametes regulates phosphorylation of the mt(+)-specific homeodomain protein GSP1. J. Biol. Chem. 274, 34383–34388. 10.1074/jbc.274.48.34383. [PubMed: 10567416]

Wong JL, and Johnson MA (2010). Is HAP2-GCS1 an ancestral gamete fusogen? Trends Cell Biol. 20, 134–141. 10.1016/j.tcb.2009.12.007. [PubMed: 20080406]

Wong JL, Leydon AR, and Johnson MA (2010). HAP2(GCS1)-dependent gamete fusion requires a positively charged carboxy-terminal domain. PLoS Genet. 6, e1000882. 10.1371/journal.pgen.1000882. [PubMed: 20333238]

Xu J (2019). Distance-based protein folding powered by deep learning. Proc. Natl. Acad. Sci. USA 116, 16856–16865. [PubMed: 31399549]

Xu JB, McPartlon M, and Li J (2021). Improved protein structure prediction by deep learning irrespective of co-evolution information. Nat Mach Intell 3, 601–+. 10.1038/s42256-021-00348-5. [PubMed: 34368623]

Yamamoto K, Hamaji T, Kawai-Toyooka H, Matsuzaki R, Takahashi F, Nishimura Y, Kawachi M, Noguchi H, Minakuchi Y, Umen JG, et al. (2021). Three genomes in the algal genus *Volvox* reveal the fate of a haploid sex-determining region after a transition to homothallism. P Natl Acad Sci USA 118. ARTN e2100712118 10.1073/pnas.2100712118.

Zhang J, Pinello JF, Fernandez I, Baquero E, Fedry J, Rey FA, and Snell WJ (2021). Species-specific gamete recognition initiates fusion-driving trimer formation by conserved fusogen HAP2. Nat Commun 12, 4380. 10.1038/s41467-021-24613-8. [PubMed: 34282138]

Zimmermann L, Stephens A, Nam SZ, Rau D, Kubler J, Lozajic M, Gabler F, Soding J, Lupas AN, and Alva V (2018). A Completely Reimplemented MPI Bioinformatics Toolkit with a New HHpred Server at its Core. J. Mol. Biol. 430, 2237–2243. 10.1016/j.jmb.2017.12.007. [PubMed: 29258817]

Highlights

- FUS1/GEX2 proteins mediate gamete adhesion in unicellular and multicellular plants
- FUS1 on *Chlamydomonas plus* gametes binds directly to MAR1 on *minus* gametes
- MAR1-FUS1 receptor pair formation is essential for gamete adhesion and fusion
- MAR1 is biochemically and functionally associated with conserved fusogen HAP2

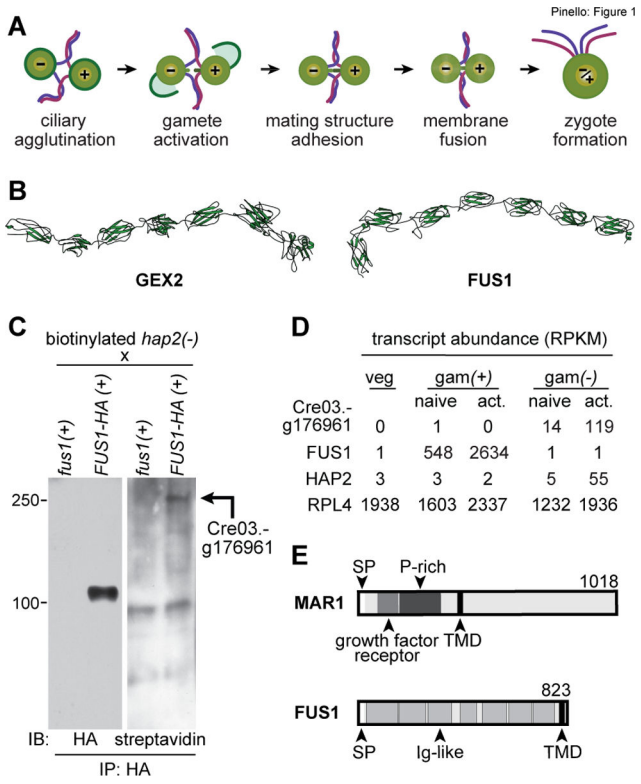

Figure 1. Relationship between FUS1 and plant sperm adhesion protein GEX2 and identification of a FUS1 binding protein in *minus* gametes.

(A) Illustration depicting steps in *Chlamydomonas* fertilization. **(B)** RaptorX structural models of the ectodomains of *A. thaliana* GEX2 (residues 28–1003) and *C. reinhardtii* FUS1 (residues 17–791). The N-terminus for each model is on the left. **(C)** *Cre03.g176961* encodes a FUS1-HA-binding protein on *minus* gametes. Immunoblots (IB) probed with anti-HA antibodies (left) or streptavidin-HRP (right) showing anti-HA immunoprecipitates (IP) of lysate supernatants from live, biotinylated *hap2(−)* gametes that had been mixed with *fus1(+)* or *FUS1-HA(+)* gametes. Mass spectrometry identified the Cre03.g176961 biotinylated protein in the FUS1-HA(+) immunoprecipitates (Data S2). **(D)** *Cre03.g176961* transcripts are specifically expressed in *minus* gametes. RPKM (Reads Per Kilobase per Million mapped reads) data from Ning et al. (2013) of the indicated transcripts (left) in vegetative cells (veg) and in naive and activated *plus* (gam(+)) and *minus* gametes (gam(−)). Results for constitutively expressed ribosomal protein RPL4 (Cre09.g397697) are also shown. **(E)** Domain architectures of MAR1 (top) and FUS1 (bottom) proteins, showing the signal peptide (SP) transmembrane domain (TMD) in each, the Ig-like folds (Ig-like) in FUS1, and the growth factor receptor cysteine-rich domain and proline-rich region (P-rich) in MAR1. (See also Table S1, Fig. S1, and Data S1, S2.)

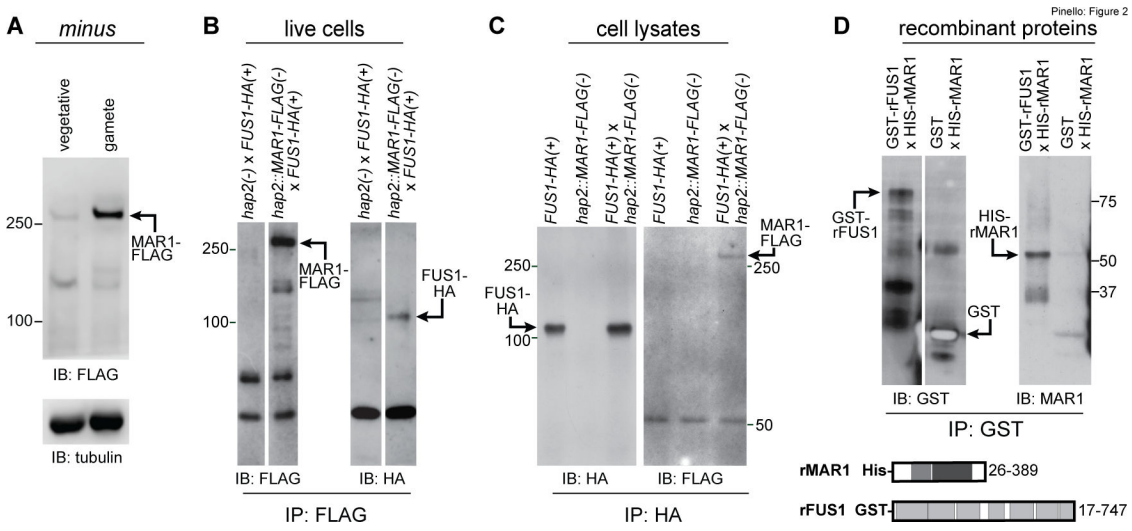

Figure 2. MAR1 on *minus* gametes directly interacts with FUS1 on *plus* gametes.

(A) MAR1-FLAG is enriched in *minus* gametes compared to *minus* vegetative cells. Immunoblot (IB) with anti-FLAG antibodies showing equal cell equivalents of *hap2::MAR1-FLAG; HAP2-HA(−)* vegetative cells and gametes (upper panel). Lower panel shows a tubulin loading control. **(B)** MAR1-FLAG interacts with FUS1-HA during mating structure adhesion. *FUS1-HA(+)* gametes were mixed for 30 min with *hap2*::*MAR1-FLAG(−)* or *hap2(−)* gametes, and lysate supernatants from the mixed gametes were subjected to immunoprecipitation (IP) with anti-FLAG antibodies followed by immunoblotting with anti-FLAG (left) or anti-HA antibodies (right). **(C)** FUS1 and MAR1 interact with each other when separately prepared cell lysates are mixed. Separately lysed mixtures of *FUS1-HA(+)* with *hap2(−)* gametes and *hap2::MAR1-FLAG(−)* with *fus1(+)* gametes were either kept separate (controls; left and middle lanes) or mixed together (right lane) and subjected to immunoprecipitation with anti-HA antibodies followed by immunoblotting with anti-HA (left) or anti-FLAG (right) antibodies (see also Fig. S2). **(D)** The recombinant GST-tagged ectodomain of FUS1 (GST-rFUS1) interacts with the recombinant His-tagged ectodomain of MAR1 (His-rMAR1). GST-rFUS1 and GST protein in bacterial lysates were bound to glutathione beads followed by incubation of those beads with lysates from bacteria expressing His-rMAR1. Proteins eluted with reduced glutathione were immunoblotted with anti-GST (upper left) or anti-MAR1 antibodies (upper right). Illustrations depicting the ectodomain residues in His-rMAR1 and GST-rFUS1 recombinant proteins (lower panel). White spaces indicate superfluous lanes digitally eliminated in blots in B and D. Protein interaction experiments were carried out at least 3 times.

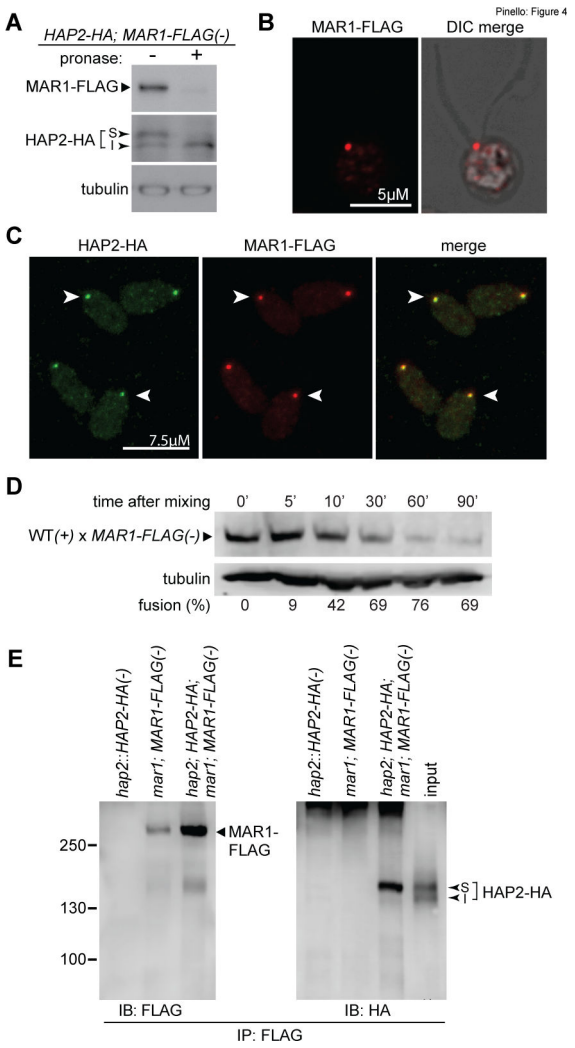

Figure 3. MAR1 is essential for mating structure adhesion and gamete fusion.

(A) Illustration of the *MAR1* gene showing the location of the disrupting CIB1 insertion cassette in the *mar1(−)* mutant (CLiP: *LMJ.RY0402.185187*). Dark grey rectangles and lines represent exons and introns, respectively. Light grey rectangles represent 5' and 3' UTRs. DNA gel electrophoresis image (lower right) shows results of genotyping PCRs across the *mar1* insertion site using primers p1 and p2 and DNA template from WT*(+)*, *mar1(−)*, and WT*(−)* cells, and a water template control. The 2.6 kB amplicons from *mar1*(−) cells were sequenced to confirm the CIB1 insertion location in the 3rd exon of the *MAR1* coding sequence (Fig. S3). **(B)** Ciliary agglutination and gamete activation are unperturbed in the *mar1(−)* gametes. Differential interference contrast (DIC) micrographs of live, WT_b*(−)* and *mar1(−)* gametes before (top) and 10 min after (bottom) mixing with WT*(+)* gametes; scale bar 0.2 mm. The large clusters of cells visible in the bottom images form when multiple cells interact with each other by their cilia. The percent of cells that lost their cell walls after mixing (4 biological replicates) is indicated below the images (± SD). **(C)** Scanning electron micrograph of *mar1; hap2(−)* gametes experiencing ciliary adhesion with WT*(+)* gametes. **(D)** *mar1(−)* gametes fail to undergo mating structure adhesion with WT*(+)* gametes. Results

are from 10 to 16 biological replicates per group analyzed using one-way non-parametric ANOVA with Dunn's post-test; **** $P<0.0001$; ns, not significant; bars are means; error bars, SD. **(E-F)** MAR1 is required for gamete fusion. Gamete fusion and zygote formation were assessed microscopically at 10 min **(E)** and macroscopically at 1–3 days **(F)** after mixing of the indicated gametes. For **(E),** results from 5 to 14 biological replicates per group were analyzed using one-way non-parametric ANOVA with Dunn's post-test; **** $P<0.0001$ and ** $P=0.0027$; bars are means; error bars, SD. Images in **(F)** are representative of one to three biological replicates. *21gr* was the WT*(+)* gamete strain used as controls in these experiments. WT*(−)* gametes used as controls were *hap2::HAP2-HA(−)* (WT_a) and parental CLiP mutant strain, *CC-5325(−)* (WT_b).

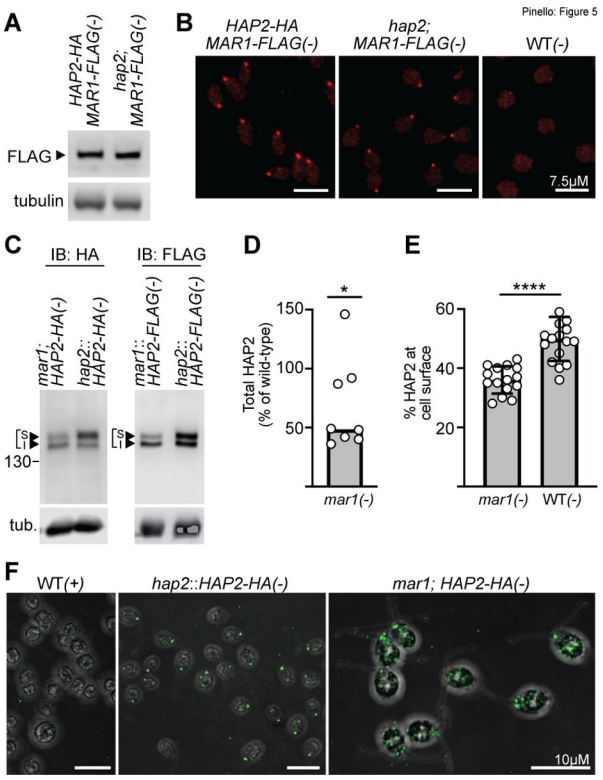

Figure 4. MAR1 co-localizes with HAP2 on the surface of the *minus* mating structure and is biochemically associated with the fusogen.

(A) MAR1-FLAG is expressed at the cell surface. Live *hap2::HAP2-HA; MAR1-FLAG(−)* gametes were incubated with or without pronase (0.05%) for 20 min followed by immunoblotting with anti-FLAG and anti-HA antibodies. The surface (S) and internal (I) isoforms of HAP2-HA are indicated. **(B)** MAR1-FLAG is localized at the *minus* mating structure at the apical end of *minus* gametes between the two cilia. Fluorescence alone and fluorescence-merged DIC single z-section images of a naive *mar1;MAR1-FLAG;hap2;HAP2-HA(−)* gamete immunostained with anti-FLAG antibodies (see also Fig. S4). **(C)** MAR1-FLAG staining is coincident with HAP2-HA at the *minus* gamete mating structure (arrowheads). *mar1;MAR1-FLAG;hap2;HAP2-HA(−)* gametes were immunostained with anti-FLAG and anti-HA antibodies. **(D)** MAR1-FLAG is rapidly lost after gamete fusion. *mar1::MAR1-FLAG(−)* gametes were mixed with WT*(+)* gametes and assayed for fusion and for MAR1-FLAG at the indicated times after mixing. The lower panel shows tubulin loading controls. Percent fusion is shown below the blots. **(E)** MAR1 is biochemically associated with HAP2. *Minus* gametes expressing both MAR1-FLAG and HAP2-HA were activated by mixing with adhesion-defective *fus1(+)* gametes for 60 min, followed by immunoprecipitation with anti-FLAG antibodies and immunoblotting with anti-FLAG (left panel) or anti-HA (right panel) antibodies. Strains lacking either MAR1-FLAG or HAP2-HA were controls; input (represents ~2.6% of the cell equivalents loaded in the eluate lane) for the *mar1;MAR1-FLAG;hap2;HAP2-HA(−)* sample is shown on the right panel. HAP2-MAR1 interaction experiments were carried out at least 4 times. Surface (S) and internal (I) isoforms of HAP2-HA are indicated.

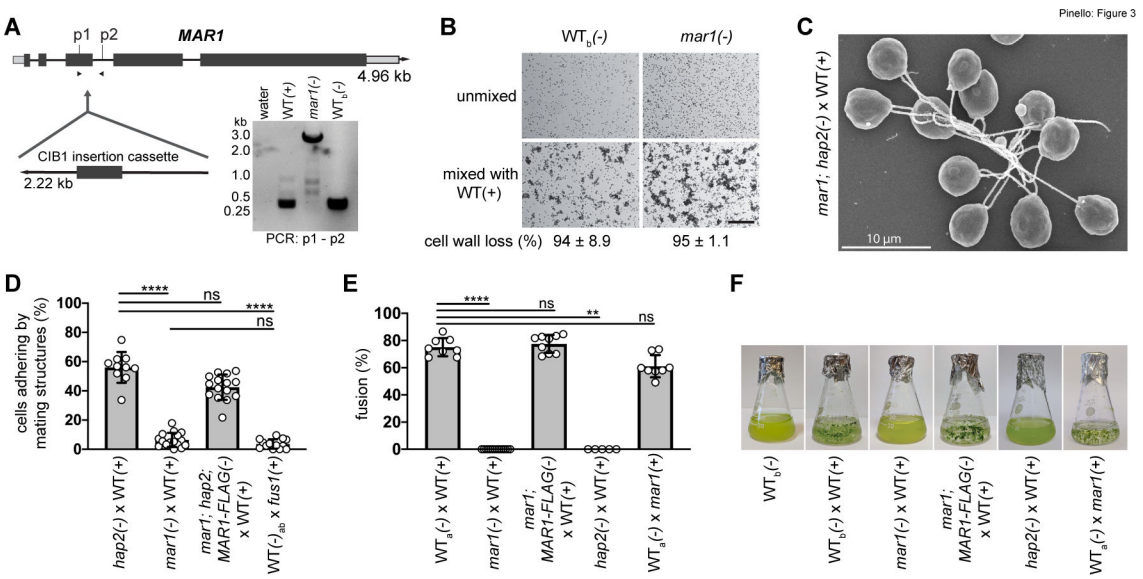

Figure 5. HAP2 expression and localization depend on MAR1, but MAR1 properties are independent of HAP2.

(A-B) MAR1 expression and localization are independent of HAP2. **(A)** Immunoblots of MAR1-FLAG (upper panel) in lysates of *mar1;MAR1-FLAG;hap2;HAP2-HA(−)* gametes (left side) and *mar1;MAR1-FLAG;hap2(−)* gametes (right side). Tubulin is shown as a loading control (lower panel). **(B)** MAR1-FLAG immunolocalization in *mar1;MAR1-FLAG;hap2;HAP2-HA(−)* gametes (left), and *mar1;hap2;MAR1-FLAG(−)* gametes (middle) by fluorescence microscopy. Negative control (right) was WT*(−)* gametes expressing neither HAP2-HA nor MAR1-FLAG. **(C-F)** HAP2 expression and mating structure localization are impaired in *minus* gametes lacking MAR1. **(C)** Representative immunoblots from lysates of HAP2-HA-expressing (left panel) or HAP2-FLAG-expressing (right panel) *minus* gametes in the absence (left lanes) or presence (right lanes) of WT *MAR1*. Controls (right lanes) were *hap2::HAP2-HA(−)* and *hap2::HAP2-FLAG(−)* gametes which contained the endogenous WT *MAR1* gene; lower panel shows tubulin (tub) loading controls. **(D)** Quantification of total HAP2-HA and HAP2-FLAG in immunoblots that was normalized to tubulin for each sample. Median HAP2 expression (bar) in *mar1(−)* gametes was 49% of that in *minus* gametes expressing WT *MAR1*; Wilcoxon Signed Rank test, **P*=0.04. Each open circle represents a biological replicate *mar1(−)* sample (*n*=8) and is expressed as a percentage of the median signal present in WT *MAR1(−)* samples (*n*=5). **(E)** Quantification of the percentage of total HAP2 present in the upper isoform of the HAP2 doublet that was determined from immunoblot signals of HAP2-HA or HAP2-FLAG expressed in *mar1(−)* or WT *MAR1(−)* gametes. The mean percent of cell surface HAP2 in *mar1(−)* gametes was 36% (*n*=15) compared to 50% in WT *MAR1(−)* gametes (*n*=17); two-tailed unpaired t test with Welch's correction; *****P*<0.0001; bars are mean; error bars, SD. **(F)** Confocal z-stack composite images of anti-HA immunostained *mar1;HAP2-HA(−)* gametes (lacking *MAR1*, right), *hap2::HAP2-HA(−)* gametes (containing WT *MAR1*, middle), and control WT*(+)* gametes (left). The HA immunofluorescence of the *mar1;HAP2-HA(−)* gametes was substantially dimmer than that of the *hap2::HAP2-HA(−)*

gametes, and the relative brightness was increased here to allow visualization of the altered HAP2-HA distribution (see also Fig. S5).

KEY RESOURCES TABLE

REAGENT or RESOURCE	SOURCE	IDENTIFIER
Antibodies		
Rat monoclonal anti-HA (clone 3F10)	Roche	Cat#11867423001 (Lot#42155800)
Mouse monoclonal anti-FLAG M2	Sigma	Cat#F1804 (Lot#SLBJ4607V)
Rabbit polyclonal anti-HA	AbClonal	Cat#AE036 (Lot#356155811)
Rabbit polyclonal anti-FLAG	Sigma	Cat#F7425
Mouse anti-HA	Santa Cruz	Cat#SC-7392
Mouse anti-FLAG (clone M2)	Sigma	Cat#F-1804
Mouse monoclonal anti-α-tubulin (B512)	Sigma	Cat#T6074 (Lot#037M4804V)
Goat anti-rat IgG HRP	EMD Millipore	Cat#AP136 (Lot#3270737)
Goat anti-mouse IgG HRP	EMD Millipore	Cat#12-349 (Lot#2985412)
Alexa Fluor 488 Goat anti-rat IgG (H+L)	Invitrogen	Cat#A11006 (Lot#2299157)
Alexa Fluor 594 Goat anti-mouse IgG (H+L)	Invitrogen	Cat#A11005 (Lot#1830459)
Alexa Fluor 488 Donkey Anti-Rat	Invitrogen	Cat#A48269
Alexa Fluor 594 Donkey anti-mouse	Invitrogen	Cat#A32744
Mouse monoclonal anti-GST	Santa Cruz	Cat#SC-138
Rabbit polyclonal anti-MAR1 (Custom-generated against MAR1 peptide: TQPPRPPWPPRPPPAPPPS, residues 164–182)	YenZym™	Rabbit#YZ5485-6 (Lot#50317)
Bacterial and virus strains		
B21 (DE3) cells	New England Biolabs	Cat#C2527I
Chemicals, peptides, and recombinant proteins		
Protease Inhibitor cocktail for Plant cell and tissue extracts	Roche	Cat#11836153001 (Lot#25765800)
Poly-l-lysine	Sigma	Cat#P8920
Fluoromount-G	Southern Biotech	Cat#0100-01 (Lot#D1810-Q490)
Prolong Gold antifade reagent	Invitrogen	Cat#P36934 (Lot#2322656)
SuperSignal West Femto Max Sensitivity substrate	ThermoFisher Scientific	Cat#34095 (Lot#WE325003)
Protein A Sepharose 4B Fast Flow from *S. aureus*	Sigma	Cat#P9424 (Lot#MKBZ075IV)
lysozyme	ThermoFisher Scientific	Cat#89833
IPTG	ThermoFisher Scientific	Cat#34060
HRP-conjugated streptavidin	Jackson ImmunoResearch	Cat#016030084
Paraformaldehyde	Aldrich	Cat#441244 (Lot#MKCB6246)

REAGENT or RESOURCE	SOURCE	IDENTIFIER
Phire Hot Start II DNA Polymerase	ThermoFisher Scientific	Cat#F-122 (Lot#00760841)
Chelex 100 Resin	BioRad	Cat#142-1253 (Lot #: 64404479)
Agar, microbiology tested suitable for plant cell culture	Sigma	Cat#A1296 (Lot#BCCD6437)
30% Acrylamide/Bis Solution 37.5:1	BioRad	Cat#1610158 (Lot#64316706)
Ammonium persulfate	Sigma	Cat#A3678 (Lot#MKBW1233V)
N,N,N',N'- Tetramethyl ethylenediamine (TEMED)	Sigma	Cat#T9281 (Lot#BCCF2825)
TCEP-HCl	GoldBio	Cat#TCEP10 (Lot#9915.052616A)
DTT	Sigma	Cat#D0632 (Lot#SLBW1508)
$HgCl_2$	ThermoFisher Scientific	Cat#M155I
OsO_4	Electron Microscopy Sciences	Cat#19140
Glutaraldehyde solution, grade II, 25% in H_2O	Sigma	Cat#G-6257 (Lot#55H0619)
Dibutyryl-cAMP	Sigma	Cat#D0627
EZ-Link™ Sulfo-NHS-LC-Biotin	ThermoFisher Scientific	Cat#21335 (Lot#QJ222159)
Pronase	Roche	Cat#10165921001 (Lot#70506922)
Trypsin from bovine pancreas	Sigma	Cat#T8003 (Lot#SLBM232IV)
Trypsin inhibitor from chicken egg white	Sigma	Cat#T2011 (Lot#SLBP7284V)
Methanol	Pharmco	Cat#339000000 (Lot#C19C12006)
Sodium orthovanadate (Na_3O_4V)	Aldrich	Cat#450243 (Lot#MKBZ693OV)
NaF	Sigma	Cat#201154
Phenylmethylsulfonylfluoride (PMSF)	Roche	Cat#15460420 (Lot#10837091001)
Gelatin from cold water fish skin	Sigma	Cat#G7765 (Lot#SLBS7921)
Goat Serum	Sigma	Cat#G9023 (Lot#SLCB4567)
Donkey Serum	Sigma	Cat#D9663 (Lot#SLCD2393)
Sodium deoxycholate	Sigma	Cat#D6750 (Lot#126K0061)
Triton X-100	Sigma	Cat#X-100 (Lot#SLBM7930V)
Transcriptor First Strand cDNA Synthesis kit	Roche	Cat#04379012001 (Lot#10769023)
DNase I	Ambion	Cat#AM2222

REAGENT or RESOURCE	SOURCE	IDENTIFIER
RNase A	Thermo Scientific	Cat#EN0531
Glutathione beads	Sigma	Cat#G4510
Glutathione, reduced	Sigma	Cat#G6013
Infusion Dry-down PCR Cloning Kit	Takara (Clontech)	Cat#639602
HA peptide	Roche	Cat#11666975001
FLAG peptide	Sigma	Cat#F4799
Experimental models: Organisms/strains		
C. reinhardtii: LMJ.RY0402.185187(−) or *mar1(−): Cre03.g176961::pCIB(−)*	CLiP Library (Li et al., 2019) https://www.chlamylibrary.org/index	LMJ.RY0402.185187
C. reinhardtii: progeny 106: *mar1(−)*	This paper	N/A
C. reinhardtii: progeny 133: *mar1(−)*	This paper	N/A
C. reinhardtii: progeny 144: *mar1(−)*	This paper	N/A
C. reinhardtii: WT*(−): cw15(−)*	*Chlamydomonas* Resource Center https://www.chlamycollection.org/	CC-5325
C. reinhardtii: CC-5313: *Cre12g541400::pSL72(+)*	*Chlamydomonas* Resource Center	CC-5313
C. reinhardtii: progeny 3d-1: *mar1;MAR1-FLAG(+)*	This paper	N/A
C. reinhardtii: MF-c7: *mar1::MAR1-FLAG(−)*	This paper	N/A
C. reinhardtii: progeny 111: *mar1;MAR1-FLAG(−)*	This paper	N/A
C. reinhardtii: progeny 115: *mar1;MAR1-FLAG(−)*	This paper	N/A
C. reinhardtii: progeny 147: *mar1;MAR1-FLAG(−)*	This paper	N/A
C. reinhardtii: progeny 73: *mar1;hap2(−)*	This paper	N/A
C. reinhardtii: progeny 98: *mar1;hap2(−)*	This paper	N/A
C. reinhardtii: progeny 148: *mar1;hap2(+)*	This paper	N/A
C. reinhardtii: progeny 156: *mar1;hap2(+)*	This paper	N/A
C. reinhardtii: FUS1-HA(+): fus1::FUS1-HA(+)	(Liu et al., 2010)	N/A
C. reinhardtii: fus1(+): imp1-15 (fus1)	*Chlamydomonas* Resource Center (Ferris et al., 1996)	CC-1158
C. reinhardtii: HAP2-FLAG(−): hap2[40d4]::HAP2-FLAG-ble(−)	*Chlamydomonas* Resource Center (Liu *et al.*, 2010)	CC-5309
C. reinhardtii: HAP2-HA(−) or WT*(−): hap2[40d4]::HAP2-HA(−)*	*Chlamydomonas* Resource Center (Feng et al., 2018; Liu et al., 2015)	CC-5295
C. reinhardtii: hap2(−): [40d4] B215.Cre16.g674852::pMN56(−)	*Chlamydomonas* Resource Center (Liu *et al.*, 2015)	CC-5281
C. reinhardtii: WT*(+): 21gr*	*Chlamydomonas* Resource Center (Proschold et al., 2005; Sager, 1955)	CC-1690
C. reinhardtii: IFT172-FLAG: fla11-2; FLAG-IFT172 (1G3)	*Chlamydomonas* Resource Center (Lin et al., 2018)	CC-5466
C. reinhardtii: IMP3-HA: imp3::IMP3-HA	*Chlamydomonas* Resource Center (Lin et al., 2013)	CC-5149
C. reinhardtii: progeny 78: *mar1;hap2;MAR1-FLAG(−)*	This paper	N/A
C. reinhardtii: progeny 146: *mar1;hap2; MAR1-FLAG(−)*	This paper	N/A

REAGENT or RESOURCE	SOURCE	IDENTIFIER
C. reinhardtii: progeny 122: *mar1;HAP2-HA (−)*	This paper	N/A
C. reinhardtii: progeny 132: *mar1;hap2;HAP2-HA(−)*	This paper	N/A
C. reinhardtii: HF-6: *mar1::HAP2-FLAG(−)*	This paper	N/A
C. reinhardtii: progeny HF-10: *mar1::HAP2-FLAG(−)*	This paper	N/A
C. reinhardtii: hap2::HAP2-HA;MAR1-FLAG(−)	*Chlamydomonas* Resource Center	CC-5284
C. reinhardtii: progeny 102: *mar1;MAR1-FLAG;hap2;HAP2-HA(−)*	This paper	N/A
C. reinhardtii: progeny 114: *mar1;MAR1-FLAG;hap2;HAP2-HA(−)*	This paper	N/A
C. reinhardtii: progeny 131: *mar1;MAR1-FLAG;hap2;HAP2-HA(−)*	This paper	N/A
Oligonucleotides		
HSV-TEV-FLAG: CAGCCAGAACTCGCCCCGGAAGACCCCGAGGATGATCGA TCCGGACCGGAGAACCTGTATTTCCAGGGAGCCATCCCC ACGACGGAGAACCTGTACTTCCAGGTGGACGCCAACTGC CGGCCCGGCTCCTCCATGGACTACAAGGACCACGATGGC GATTACAAGGATCACGACATCGACTACAAGGACGACGAC GACAAG	This paper	N/A
p1 Mar1_185187_F2 genotyping: CACCGCCTGGAACTACTCCTC	This paper	N/A
p2 Mar1_185187_R2 genotyping: TTGGGTCTGGTTTAGATTTGGGCTGG	This paper	N/A
RB1 CC-5313 genotyping: ATGGGGCGGTATCGGAGGAAAAG	This paper	N/A
C12g541400.R2 CC-5313 genotyping: TGTAGCAAGGCTCCCGCTTCTAGTTG	This paper	N/A
Zeo_F1 zeocin genotyping: GCTGCATGTGCACAGTCACGCTGTCTC	This paper	N/A
Zeo_R1 zeocin genotyping: GGATCCCACACACCTGCCCGTCT	This paper	N/A
Fus1_P3_Fw *plus* gamete genotyping: GACCATCGTAGAGCGCTCTCACCAATTG	This paper	N/A
Fus1_P3_Rev *plus* gamete genotyping: CCGCTACGCTTCTGCGTCTTGATAGTC	This paper	N/A
Nit_p1_F *hap2-2* genotyping: GGTCGAGGTGCCGTAAAGC	This paper	N/A
Nit_p2_R *hap2-2* genotyping: CCTGATGCCCCTTCAACCG	This paper	N/A
L8 *MAR1* gene amplification: CGGCGGCTTTGTTCCGTTTGTTTG	This paper	N/A
R5B *MAR1* gene amplification: CAGTCTGCGTTTCCCTTCTCGTGG	This paper	N/A
G176961.R20 *ble* insertion into *MAR1-FLAG:* CCGCGAATTCactagtGCTGCATGTGCACAGTCACGC	This paper	N/A
L20 *ble* insertion into *MAR1-FLAG:* GCCCCGTGCTcctaggGGATCCCACACACCTGCCC	This paper	N/A
PGenD.s *ble* insertion into *HAP2-FLAG:* actagtGGATCCCACACACCTGCCCGTCTG	This paper	N/A
PGenD.as *ble* insertion into *HAP2-FLAG:* tctagaGCTGCATGTGCACAGTCACGCTGTCT	This paper	N/A

REAGENT or RESOURCE	SOURCE	IDENTIFIER
g176961-L3 *HIS-MAR1:* TCCGGACTTGCCTTTTTAGC	This paper	N/A
g176961-R10 *HIS-MAR1:* GGCTTCCTACAGGCCCACCA	This paper	N/A
Recombinant DNA		
Plasmid. *pGenD-Ble*	*Chlamydomonas* Resource Center (Fischer and Rochaix, 2001)	https://www.chlamycollection.org/
pGEM-T-easy vector, *MAR1*	Promega	Cat#A1360 (Lot#219942)
PET28a(+) vector, *HIS-MAR1*	GenScript assisted in cloning, see Supplemental Data S3	N/A
Plasmid. *HAP2-HA: pYJ36*	(Liu et al., 2008)	N/A
Plasmid. *HAP2- FLAG: C2925/pYJHSVTEVFL-zeo*	This paper	N/A
Plasmid. *pGEX-2T empty vector*	Sigma	Cat#GE28-9546-53
Plasmid. *GST-rFUS1: pGEX-2T FUS1*	(Misamore et al., 2003)	N/A
Plasmid. *MAR1-FLAG: DH5 α/pYJFUS1BHSVFL+Z*	This paper	N/A
Software and algorithms		
Leica LAS X core module	Leica Microsystem Inc.	https://www.leica-microsystems.com
StreamPix 5.8.1.0	NorPix	https://www.norpix.com/products/streampix/streampix.php
GraphPad Prism Version 9.0.0	GraphPad	https://www.graphpad.com/
Image Studio™	LI-COR	https://www.licor.com/bio/image-studio/
PyMol Software	Schrodinger, LLC	https://www.schrodinger.com/products/pymol
Adobe Illustrator and Photoshop	Adobe	https://www.adobe.com/products/catalog.html
RaptorX	(Källberg et al., 2012; Xu, 2019; Xu et al., 2021)	http://raptorx.uchicago.edu/
PROMALS3D	(Pei and Grishin, 2007)	http://prodata.swmed.edu/promals3d/promals3d.php
DELTA-BLAST	(Boratyn et al., 2012)	https://blast.ncbi.nlm.nih.gov/Blast.cgi?PAGE_TYPE=BlastSearch&PROGRAM=blastp&BLAST_PROGRAMS=deltaBlast
PSI-BLAST	(Altschul et al., 1997; Aravind and Koonin, 1999)	https://blast.ncbi.nlm.nih.gov/Blast.cgi?PAGE_TYPE=BlastSearch&PROGRAM=blastp&BLAST_PROGRAMS=psiBlast

REAGENT or RESOURCE	SOURCE	IDENTIFIER
PHYRE2	(Kelley et al., 2015)	http://www.sbg.bio.ic.ac.uk/phyre2/html/page.cgi?id=index
SWISS-MODEL	(Waterhouse et al., 2018)	https://swissmodel.expasy.org/
HHPRED	(Zimmermann et al., 2018)	https://toolkit.tuebingen.mpg.de/tools/hhpred